# Exosomes as Hedgehog carriers in cytoneme-mediated transport and secretion

Ana-Citlali Gradilla[1], Esperanza González[2#], Irene Seijo[1#], German Andrés[1#], Marcus Bischoff[3], Laura González-Mendez[1], Vanessa Sánchez[1], Ainhoa Callejo[1], Carmen Ibáñez[1], Milagros Guerra[1], João Ramalho Ortigão-Farias[1], James D. Sutherland[2], Monika González[2], Rosa Barrio[2], Juan M. Falcón-Pérez[2,4,5*], Isabel Guerrero[1*].

1- Centro de Biología Molecular "Severo Ochoa" (CSIC-UAM), Nicolás Cabrera 1, Universidad Autónoma de Madrid, Cantoblanco, E-28049 Madrid, Spain.

2- CIC bioGUNE, Bizkaia Technology Park, 48160 Derio, Spain.

3- University of St Andrews, Biomedical Sciences Research Complex, North Haugh, St Andrews, Scotland, KY16 9ST, UK

4- IKERBASQUE, Basque Foundation for Science, 48011, Bilbao, Spain.

5- Centro de Investigación Biomédica en Red de Enfermedades Hepáticas y Digestivas (CIBERehd), Bizkaia Technology Park, 48160 Derio, Spain.

*Corresponding authors: iguerrero@cbm.uam.es, Phone: +34 91 196 4680/4465

jfalcon@cicbiogune.es, Phone: +34 944 061 319/219

# Equal contribution.

**Running Title:** Hedgehog secretion in exovesicles.

**Key words:** Hh signalling, exosomes, cytonemes, cell-to-cell communication, Hh dispersion

**ABSTRACT**

**The Hedgehog signalling pathway is crucial for development, adult stem cell maintenance, cell migration, and axon guidance in a wide range of organisms. During development, the Hh morphogen directs tissue patterning according to a concentration gradient. Lipid modifications on Hh are needed to achieve graded distribution, leading to debate about how Hh is transported to target cells despite being membrane-tethered. Cytonemes in the region of Hh signalling have been shown to be essential for gradient formation, but the carrier of the morphogen is yet to be defined. Here we show that Hh and its co-receptor Ihog are in exovesicles transported via cytonemes. These exovesicles present protein markers and other features of exosomes. Moreover, the cell machinery for exosome formation is necessary for normal Hh secretion and graded signalling. We propose Hh transport via exosomes along cytonemes as a significant mechanism for the restricted distribution of a lipid-modified morphogen.**

**INTRODUCTION,**

The Hh molecule acts as a morphogen to regulate growth and cell fate specification at a distance. In different systems Hh is secreted from a restricted group of cells and distributed in a concentration-dependent manner according to distance from the source, resulting in differential activation of target genes[1]. Thus, Hh production, release, transport and reception must be kept under strict spatial and temporal control to accomplish an activity gradient. Hh gradient formation mechanisms have been studied extensively in the *Drosophila* wing imaginal disc comprising two cell populations with different adhesion affinities dividing the field into a posterior (P) and an anterior (A) compartment. The P compartment cells produce Hh, which moves across the A/P compartment border, decreasing in concentration as it spreads away from the border to the A compartment. Hh is post-translationally modified by the addition of cholesterol[2] and palmitic acid[3]

which promote Hh association to lipid membranes but are essential for its restricted spreading[4], raising the question of how its actual secretion and transfer are achieved. In both the wing disc and the abdominal epidermis of *Drosophil*a, specialized filopodia called cytonemes[5] are crucial for establishment of the Hh gradient[6]. Cytonemes are easily visualized by confocal microscope in the basal part of the wing disc epithelium by expressing the Hh co-receptor Ihog[6-8], which also labels punctate structures[8] with a size 0.1 - 0.6 μm; some of them seem to exceed the cytoneme diameter, suggesting they could be extracellular vesicles (EVs)[6]. In the chicken limb bud, particles containing SonicHh (SHh) and CDO (vertebrate homologue of Ihog) have also been shown to travel along filopodia-like extensions within the field of SHh signalling[9]. Here we characterize these structures and their association with Hh, determining the role of EVs in Hh distribution and gradient formation.

## RESULTS

### Hedgehog is located in EVs that move towards recipient cells

In the wing disc, Hh punctate structures (endogenous or ectopically expressed Hh-GFP) locate at the plasma membrane both apically and basolaterally (Fig. 1B), and in both P and A compartment cells near the A/P border[1] (Fig.1C). Importantly, these puncta can be partially labelled by extracellular *ex vivo* staining with anti-GFP antibody (Fig.1 B-C), indicating the presence and the extracellular localization of Hh on their surface. They are more abundant at the basolateral part of the disc epithelium (Fig 1 B,C red and yellow puncta), and distinct from cytoplasmic puncta[8] (green puncta in Fig. 1C).

Co-expression of Hh-GFP and Ihog-RFP reveals puncta labelled with both markers in the A compartment, as well as puncta that just contain Hh-GFP probably due to internalization of Hh-GFP vesicles by the receiving cells (Fig. 1D, see also Supplementary Movie 1). Live imaging of Ihog-RFP puncta in the abdomen, where Hh also acts as a morphogen[10], confirms their presence

both laterally as well as basolaterally, similar to Hh (Supplementary Movie 2). Disp[11] and Dlp[8], both essential for Hh release[8], also co-localize with Ihog-labelled punctate structures and cytonemes (Fig. 1E-G). These results indicate that Hh could indeed be transported in extracellular vesicles (EVs) together with other pathway components, Ihog, Disp and Dlp, all involved in Hh release. The punctate structures localize to cytonemes in the basal side of the epithelium[6]; and as *ex-vivo* antibody staining marks both Disp and Hh, these proteins might all be at the surface of EVs (Supplementary Fig. 1G).

To further investigate the EV nature of the puncta, immuno-labelling for Hh in wing discs co-expressing Ihog-RFP and the mammalian EV marker CD63 tagged with GFP[12] was performed, revealing a clear co-localization of the three in punctate structures (Fig. 2A). This co-localization was also confirmed by live imaging in the abdominal epidermis of pupae co-expressing CD63-GFP and Ihog-RFP (Fig. 2B and Supplementary Movie 3). Furthermore, immunoprecipitation of the GFP-tagged CD63 shows co-immunoprecipitation of Ihog-RFP and endogenous Hh *in vivo* (Fig. 2C-E), supporting the presence of CD63 in the Hh-Ihog complex observed by confocal imaging and strongly advocating the EV nature of the puncta (Fig. 2A-B).

Detailed observation of movies with CD63-GFP marked puncta shows their association with cytonemes in basal regions, where they move along the cytonemes which point from the P towards the A compartment (Fig.3 A-B and Supplementary Movie 4 and 5). Live imaging of cells expressing either the membrane marker CD4-Tomato or Ihog-RFP also shows punctate structures moving along cytonemes (Fig. 3C-D and Supplementary Movie 6 and 7, see also[6]). Interestingly, CD4-Tomato labelling occasionally shows buckling followed by a swelling structure which might be related to direct shedding of vesicles from the cytoplasmic membrane (Fig.3C and Supplementary Movie 6), also sporadically observed in puncta labelled with Ihog-RFP (Fig. 3D and Supplementary Movie 7).

**Hh in MVBs, plasma membranes and EVs by Immuno-EM**

To analyse the distribution of Hh at the ultra-structural level, immunoelectron microscopy (Immuno-EM) was performed on thawed cryosections of wing discs expressing Hh-GFP. Supplementary Fig 1 (A-F) shows correlative light-electron microscopy of the Hh distribution on ultrathin cryosections cut orthogonal to the ventral/dorsal axis. Immunofluorescent Hh staining (Supplementary Fig. 1A) was detected along the whole apical disc lumen and at the basolateral region of the P compartment. At the EM level, apical Hh signal was found on microvilli membranes (Supplementary Fig. 1B) whereas basolateral staining on Hh producing cells was mainly detected within multivesicular bodies (MVBs) and lysosomes as well as on the basolateral membranes (Supplementary Fig. 1C,D,E). Interestingly, Hh staining was also detected on heterogeneous vesicle-like structures (size ranging from 30 to 200 nm) in basolateral extracellular spaces close to the basal lamina (Supplementary Fig. 1F,f). To further explore the extracellular distribution of Hh, wing discs expressing Hh-GFP were labelled *ex vivo* with an anti-GFP antibody before EM processing. As shown in Fig. 4A, thawed cryosections labelled with a dual fluorescent and electron-dense Fab´fragment probe showed apical staining and a basolateral punctate fluorescent pattern at the P compartment, fully consistent with the punctate labelling of external Hh observed at the confocal microscope (Fig. 1). In addition, at the EM level, immunogold staining detected Hh-GFP on apical microvilli membranes (arrows in Fig. 4B-B1) as well as on discrete regions of basolateral membranes (arrows in Fig. 4C-D), frequently associated with cell-to-cell contacts (arrows in Fig. 4D). Importantly, significant Hh labelling was detected on clusters of vesicle-like structures at the basolateral extracellular spaces (arrows in Fig. 4C, E and F) and some of these vesicles appear also localized in association with cell protrusions (arrows in Fig. 4E, insets). Finally, Immuno-EM confirmed the presence of Hh, Ihog and Disp at MVBs and exovesicles (Supplementary Fig. 1G,H, I) in cryosections of wing discs expressing Ihog-CFP and Disp-YFP, respectively. Altogether, these results support the notion that all these Hh signalling pathway components share the same secretion mechanism in exovesicles at basolateral spaces.

Due to the size of some of these EVs (30-150 nm) and their association with MVBs, they could comprise *bona fide* exosomes[13], defined as extracellular vesicles enriched in cholesterol, sphingomyelin, ceramide and components of membrane raft microdomains[14]. Exosomes originate from MVBs and are released to the extracellular space following fusion with the plasma membrane, containing proteins implicated in trafficking, membrane fusion and signalling[15]. Hh has been shown to traffic from apical to basolateral plasma membranes[6-8] and this recycling process might actually localize Hh in MVBs. Both processes, Hh release[8] and MVB formation, require Rab5, Rab4, and Rab8 function[16,17].

**Hh-loaded exovesicles in culture cells**

Further characterization using *Drosophila* cultured wing disc cells, Cl8, as well as transfected S2 cells expressing Hh-GFP also show the presence of endogenous Hh or Hh-GFP in EVs. These EVs have exosome-like features based on flotation density and protein markers (Fig. 5 and Supplementary Fig. 2A-B). Characterization of the vesicular fraction by isopynic density gradients shows co-fractioning of the Hh protein with membrane (TSG101, Rab11, Rab8 and Syntaxin), and luminal (Hsp70) exosomal associated proteins[18] (Fig. 5B) and the Hh co-receptor Ihog (Supplementary Fig. 2C). Previously, it has been described that Hh is associated to lipoproteins (*Drosophila* apoliproteins; Lipophorins (Lp-I and Lp-II[19]) for transport[12]. Lp-II has also been detected in EV preparations in the presence of fly extracts (source of Lps in the *Drosophila* cell culture medium) but Lp-II does not co-fractionate with Hh-containing exosomes (Fig. 5A,B). Moreover, Hh loaded EVs were able to activate the *Ptc::luciferase* reporter (Fig. 5C-D), further showing that the Hh protein present in these EVs is functional.

Finally, interfering with proteins involved in the production/secretion of EVs, TSG101 and Rab27[20-22] in *Drosophila* wing disc cells (Cl8 cells) leads to a significant reduction in the levels of Hh protein associated to EVs (Supplementary Fig. 2D). However, in our *in vitro* model,

interference with the ESCRT independent exosome production protein nSMase does not show a significant decrease in the Hh levels within EVs (Supplementary Fig. 2D). Together, results obtained from cell cultured EV analysis support the notion that at least a fraction of functional Hh is secreted in exosome-like vesicles in *Drosophila* cells.

**Exovesicle formation genes are needed for Hh release *in vivo***

From an *in vivo* perspective, preliminary observations have shown a reduction of the Hh gradient when blocking EVs formation via RNAi treatment[6]. Further, *in vivo* RNAi screening confirmed the previously observed role of genes involved in EV formation and release, identifying new proteins involved in the graded secretion of Hh via EVs. Five RNAi treatments show an effect on the Hh gradient by the analysis of the *Ptc::GFP-Enhancer-Trap* expression, a recognized reporter for both, short- and long-range Hh responses: the ESCRT complex components Vps22 (ESCRT-II component) and Vps24 (ESCRT-III component), the ESCRT independent sorting protein SMase[23], the SNARE complex component Ykt6 and the *Drosophila* homologous for the P4-ATPase (CG31729), TAT-5 in *C. elegans* shown to regulate the budding of EVs from the plasma membrane (shedding vesicles/ectosomes/microparticles)[24] (Fig. 6A a-d). All these proteins are involved in EV secretion pathways and Ykt6 has also been shown to be involved in the release of exosomes containing Wingless (Wg)[25]. In addition, in order to confirm the requirement of EV formation during Hh signalling, we have quantified the effect of knocking down a fraction of the genes identified over the long-range target Cubitus interruptus (Ci), and a significant decrease in activation was also observed (Fig 6A e-h). These experiments then endorse the necessity of the molecular machinery for EV formation and release for both short- as well as long-range Hh signalling.

To further analyse the effect of knocking down EVs production genes over Hh-loaded EVs *in vivo*, we ectopically expressed Hh-GFP or Ihog-RFP in producing cells, quantifying the

visible punctate structures only in the A compartment (Fig.6B and for methods Supplementary Fig 3). We tested RNAi treatments with a clear effect in Hh signalling (Fig. 6A and[6]) including the ESCRT-0 protein Hrs[26], the accessory ESCRT protein ALiX[26], the EV component Anx B11[27], the endosomal sorting protein Rab11 implicated in EV targeting[28], and the lipid raft component Flo2 also found in EVs[29]. All RNAi treatments tested result in significantly fewer Hh-GFP puncta in the A compartment (Fig. 6Ba-c), showing an effect on actual Hh secretion. Similar reduction effects were also observed for Ihog-RFP puncta, confirming again the role of these genes in the regulation of the Hh pathway (Fig 6Bd). Moreover, interfering with EV production decreases the externalized levels of endogenous Hh (see Fig 6Cc expressed in levels of ratio change), shown by e*x vivo* staining after depletion only in the dorsal compartment of the disc while the ventral part retains wild type conditions (Fig. 6C a-b). Importantly, all RNAis used did not have a significant apoptotic effect after treatment (Supplementary Fig. 4A). In addition, quantitative RT-PCR experiments for four of these treatments confirmed the significant reduction of targeted RNA levels induced by the RNAis expression (Supplementary Fig.4B).

On the other hand, immunolabelling for total endogenous Hh levels of wing discs expressing the RNAi constructs only in the dorsal compartment, and compared to the wild type ventral compartment, show no significant change, excluding potential effects of RNAi treatments over production or degradation of intracellular Hh (Supplementary Fig. 4C). The only exceptions to the latter observation were the RNAi treatment for the ESCRT-I component TSG101 and the ESCRT-II component Vps22, which show significant accumulation of total Hh on the P compartment (paired t-test, $t = -5.19$, $df = 7$, $p<0.01$) (Supplementary Fig. 4Cc). However, despite this accumulation both TSG101 and Vps22 RNAi treatment still lead to a reduction in the extracellular levels of Hh (Fig. 6C). Thus, and taking into account all data from RNAi treatments, EV production is required for the normal release levels of Hh to the extracellular space in the wing disc and consequently for the normal graded signalling pattern.

## DISCUSSION

Our previous research showed a requirement for cytonemes extending from Hh producer cells towards receptor cells for Hh gradient formation, while Hh was also observed in punctate structures[6]. Here, we characterized these puncta confirming their EV nature and role during Hh signalling. These Hh-loaded exovesicles are a heterogeneous group, differing in size and potentially in origin. *In vivo* imaging shows puncta moving along cytonemes, suggesting a route of Hh secretion and restricted dispersion where Hh-containing EVs are transported by cytonemes. Nevertheless, to date we still do not know the precise mechanism used for Hh release and transport along the cytoneme. Ultrastructural analysis confirmed the presence of Hh in MVBs on the A compartment, supporting an ESCRT dependent route of exovesicle formation and release. Thus, it is possible that MVBs fuse to the plasma membrane releasing vesicles at the same time as cytonemes are elongating, and that these smaller vesicles either travel within the cytoneme (that could be small MVBs) or on the cytoneme. However, live imaging of these structures also shows puncta shedding directly from the cytonemes, and these might correspond to membrane-derived vesicles known as shedding vesicles or ectosomes/microvesicles[30].

Ectosome EVs were described as bigger than exosomes and more heterogeneous in size, ranging from 200 nm to greater than 1 μm in diameter, and are originated by shedding preceded by the budding of small cytoplasmic protrusions, which then detach by fission of their stalk[30]. Although shedding vesicles/ectosomes seem to have a different origin[31], the mechanisms of their sorting process remain obscure and might also be dependent on the ESCRT complex[24]. In addition, studies have shown a crucial role for cholesterol-rich microdomains of the plasma membrane for shedding vesicle formation[32] as well as for biogenesis of exosomes[14]. In our *in vivo* experiments, we have observed a decrease in Hh signalling by knocking down Vps22, an ESCRT-II complex component described as dispensable for vesicles derived directly from the plasma membrane[33,34], but required for MVB formation[35] (reviewed in [36]) supporting an MVB

fusion origin. However, we have also observed a decrease in signalling and Hh release when interfering with P4-ATPase (CG-31729), the *Drosophila* ortholog of TAT-5 specifically involved in the formation of ectosomes in *C. elegans*[24]. Thus, as it is difficult to account for the considerable differences between the two types of vesicles, the result of knocking down Vps22 and P4-ATPase together with the EM data and the *in vivo* imaging indicate that Hh might be released in both ectosomes/microvesicles and exosome-like vesicles. Determining which process might be the main one regulating Hh secretion or whether both processes are linked is a future challenge.

*In vitro*, functional tests demonstrate that Hh loaded exovesicles fractionate together with classical exosomal markers (Fig 5B), and are able to activate Hh dependent transcription in cell culture (Fig 5D). Furthermore, interference with genes involved in the formation and release of EVs *in vivo* has a decreasing effect on the release of Hh to the extracellular space, altering the Hh gradient formation during signalling (Fig 6). In our experimental model (the *Drosophila* wing imaginal disc) all RNAi treatments behave similarly, independently of their individual function within the EVs formation pathways. The only exceptions were given by the silencing of ESCRT-I component TSG101 and the ECRT-II component Vps22, which resulted in a significant accumulation of total Hh in the P compartment (Supplementary Fig. 4C) but still impaired Hh secretion to the A compartment (Fig. 6B,C); probably due to a simultaneous impairment of the route for Hh degradation as they both play a key role in MVB formation[26,35]. Differential outputs after down regulation of different EVs formation genes have been reported, including an increment in EVs release (eg ALiX RNAi)[26]. However, there is increasing evidence of the heterogeneous nature of EVs in size, protein content and origin[18]. Depletion of a gene involved in the formation pathway might either affect EVs release in general or might alter the proportion of the different vesicles formed[26]. Thus, quantifying the effects over those vesicles containing Hh or Ihog might not detect potentially distinct changes in the distribution of different size vesicles or protein content.

Association of Hh to EVs and thus membranes supports the transport mechanism initially proposed by Greco et al[37] for the spread of Wg protein; Wg secreted and moved while contained in membrane fragments called argosomes. Vesicular release of SHh has also been described in the determination of left-right asymmetry in vertebrates[38]. Moreover, Hh has been found in exosomal structures for its apical secretion in *C. elegans*[39]. We have found a functional Hh associated to heterogeneous EVs, either originated from MVBs or/and directly shedding from the plasma membrane of cytonemes, and that are essential for Hh gradient formation.

Recent reports also show Wg and Wnt to be released in exosomes at the wing disc, in the zebrafish and tissue culture cells[21,22,25,40]. During patterning of the zebrafish neuroectoderm, Wnt8a localizes to membrane-associated punctate structures in live tissue and these puncta are found on filopodial cellular processes[40]. In *Drosophila*, Wg has also been visualized *in vivo* moving along cellular extensions by Evi-exosomes[18] or released as exosomes from MVBs at synaptic terminals[22]. The release of exosomes and further activation of the Hh pathway in an epithelium might then require a synaptic process with a potential complex association of various proteins. Thus, *in vitro* experiments with cultured cells might not be able to reproduce the signalling process in an epithelium, leading to the relatively low representation of Hh in exosomes and Hh dependent transcription activation.

Overall, our results support a route for morphogen transport that involves vesicle transport and secretion along cytonemes to accomplish proper spatially restricted signalling. Still, key unanswered questions regarding the final transfer or release of morphogens like Hh remain. Supporting a conserved mechanism in vertebrates, SHh and CDO (vertebrate homologue of Ihog) in vesicle-like structures have been observed moving along specialized filopodia in the chick limb bud[9]. Further elucidation of the origin, structure and function of the EVs implicated in this process as well as the mechanism of their release is likely to be essential to understand Hh cell-cell signalling. However, our results do not totally exclude a potential combinatorial effort with

other secretion routes or extracellular forms of Hh, such as lipoprotein particles[12,41] or Hh multimers[42]. Comprehending how signalling molecules like Hh are distributed will improve knowledge of developmental processes and their role in diseases like cancer, revealing a wider set of mechanisms and genes involved in the regulation of their signalling.

## METHODS

### Fly mutants.

A description of mutations, insertions and transgenes (Supplementary Table 1) is available at Fly Base (http://flybase.org/). Gal80$^{ts}$, FLP122 (Bloomington *Drosophila* Stock Centre (BDSC), Indiana, USA; http://flystocks.bio.indiana.edu).

### Overexpression experiments

The *Gal4* drivers were: *hh.Gal4*[44], *ap.*Gal4 [45], *tub*.Gal4 (BDSC). The *pUAS*-transgenes were: UAS.Hh-GFP[46], UAS.lhog-RFP[8], UASCD63-GFP[12], and UAS.*CD4-tdTom*[47].

UAS-RNAi lines targeting TSG101 (35710), ALiX (33417), Hrs (33900), Rab27 (37774), Vps 22 (38289), Vps 24 (38281), αSmase (25283) and Ykt6 (38314) were all from BDSC. Flo2 (31525), AnxB11 (29693), Rab11 (108382), P4-ATPase (CG31729) (105987) and Vps4 (105977) were from the IMP Vienna *Drosophila* RNAi Centre (VDRC; http://stockcenter.vdrc.at). 30 hours of transient expression of the UAS-constructs using Gal4; Tub-Gal80$^{ts}$ drivers was achieved by maintaining the fly crosses at 18ºC and inactivation of Gal80$^{ts}$ at the restrictive temperature (29ºC) before dissection.

### Immunostaining of imaginal discs

Immunostaining was performed according to standard protocols[48]. Imaginal discs from third instar larvae were fixed in 4% paraformaldehyde/PBS for 20 min at room temperature (RT) and washed in PBT before incubating with PBT 0.2% BSA for blocking (1 hour at RT) and primary antibody

incubations (overnight at 4°C). Incubation with fluorescent secondary antibodies (1/200 Jackson laboratories and Invitrogen) was performed for 2 hours at RT for posterior washing and mounting in mounting media (Vectashield). Antibodies were used at the following dilutions: rabbit polyclonal anti-Hh (1:800 or 1:500, raised in this work); rat monoclonal anti-Ci[50] (1:20 dilution, a gift from B. Holmgren); rabbit polyclonal anti-GFP antibody (1:500, Molecular Probes, A-6455); and rabbit polyclonal anti-Caspase 3 antibody (1:50 dilution, Asp-175 from Cell Signalling). The protocol for the *ex-vivo* labelling using anti-GFP antibody is described in[46]. Imaginal discs from third instar larvae were dissected on ice, transferred immediately to ice-cold M3 medium containing anti-Hh (1:30 dilution; rabbit antibody raised for this work), or anti-GFP (1:50 dilution, rabbit antibody A-6455; Invitrogen), or anti-Disp[8] (1:50 dilution, guinea pig antibody), or anti-Dlp (1:5 dilution; mouse antibody, Hybridome bank, Iowa) antibodies and incubated at 4°C for 30 minutes. The incubation with the primary antibody under these `in vivo' conditions, without detergents prior to fixation, rendered the antibody incapable of penetrating the cells. They were then washed in ice-cold PBS, fixed in PBS 4% PF at 4°C, washed in PBT and incubated with secondary fluorescent antibody as above.

**_In vivo_ imaging of the abdomen**

Pupae were filmed through a window in the pupal case and analysed as described previously[6]. White prepupae were attached to double-sided adhesive tape to remove the operculum with forceps. The prepupa was removed from the adhesive in a solution of 1 mM levamisole in water and moved to a new slide mounting between three bands of Parafilm “M” arranged in a U-shape to ensure minimal squashing. A total of 30 μl of 1 mM levamisole was used to surround the prepupa. A coverslip was placed over the sample, and the open part of the chamber was filled with 100 μl voltalef oil to ensure an oxygen supply. All imaged flies developed into pharate adults and many hatched. Z-stacks of around 40 μm with a step size of 2.5 or 3 μm were recorded every 150-180 seconds using a Leica SP8 confocal microscope at room temperature.

Number (*N*) of recorded pupae: Supplementary movie 2+7, *N* = 8; Supplementary Movie 3, *N* = 3; Supplementary Movie 4+5, *N* = 9; Supplementary Movie 6, *N* = 6.

**Microscopy and image processing of imaginal discs**

Laser scanning confocal microscopes (LSM510 or LSM710 Vertical; Zeiss) were used for confocal fluorescence imaging of imaginal discs. ImageJ software (National Institutes of Health) was used for image processing and for determining fluorescence levels.

**Quantification of EVs and Hh levels**

Vesicle number (Fig. 6B) was quantified using ImageJ. A defined rectangular area of 170x75 μm was chosen, which was located in the A compartment in the vicinity of the P compartment (Supplementary Fig. 3A,B). The edge limit of the P compartment cells was defined after blurring of the projected image and by creating a shaped selection to delimit edges (Supplementary Fig. 3a,b) also confirmed by the immuno-labelling of the A compartment Ptc expression (Supplementary Fig. 3C). Within the selection a mean filter of 1 pixel radius was used to smooth the image and remove noise. To remove particles that were of low fluorescence intensity, the lower threshold for pixel intensities was set to 60, whereas the upper was kept at 255. Finally, the "Analyse Particles" tool was used to count puncta within 0-4.5 pixels of size (Supplementary Fig. 3a,b). Quantifications were performed using individual Z slices taken every 1μm. All images were treated identically. For all RNAi treatments a control for potential cell death due to RNAi treatment was performed by immune-staining with anti-Caspase antibody (see Supplementary Fig. 4A); no significant increment of cell death due to treatment was detected.

Levels of externalized Hh (Fig. 6C) and total Hh (Supplementary Fig. 4C) were quantified by determining the Mean Gray Value in ImageJ. A rectangular area of approximately 14,400 pixels within the wing pouch on each side of the dorso-ventral border marked by GFP expression driven by the *ap.*Gal4 was used.

**Quantification of gradient length**

Gradient lengths were determined as described in [6] and then expressed as a proportion of the wing pouch length (Fig. 6 A).

**Quantitative RTqPCR**

The RNAis' ability to down regulate their target genes in the transgenic flies was already tested by the manufacturer (BDSC Trip toolbox stocks). Four RNAi treatments were tested (Supplementary Fig. 4B). Three independent biological replicate assays were produced for TSG101-, Flo2-, Rab11-, and the control EGFP-RNAi constructs, and six replicates in the case of HRS- and its control EGFP-RNAi. For RNA extraction *Drosophila* third instar larvae expressing RNAi constructs or not were collected and kept at -80ºC. Larval tissues were homogenized in 500μl Trizol (Invitrogen), 100μl Chloroform (Merck). After a 15 min 12000 rpm centrifugation at 4ºC the upper phase containing total RNA was collected and precipitated with 250μl 2,3-propanol (Merck). The dry pellets were resuspended in 40μl sterile water and stored at -80ºC. For the *RT-qPCR* reaction, RNA concentration was measured using the Nanodrop ND-1000 and RNA integrity was confirmed using the "Total RNA Analysis ng sensitivity (Eukaryote)" assay of the Agilent 2100 bioanalyzer. cDNA was generated using Super Script III First-Strand Synthesis SuperMix for qRT-PCR from Invitrogen (PN 11752250), 800 ng of total RNA were used for each replicate in a final volume of 20 ul (final concentration of 40 ng/μl). qPCR reactions (95°C for 10 min., followed by 40 cycles of 95°C for 15sec. and 60°C for 30sec.; and 1 cycle of 95ºC for 15sec, 60ºC for 15sec and 95ºC for 15sec) were run on the CFX 384 (Biorad) according to the manufacturer's instructions.

*Primers used in RTqPCR:*

**Flo2_1F** 5'-GGCGATGCAGCAATTATGA-3', **Flo2_1R** 5'-TCATCGGTTTTGGCCAGT-3',

**Flo2_2F** 5'-GACGCAAGCAGATCGAGATT-3', **Flo2_2R** 5'-GATGGTCTGACATTGCTTGG-3',

**Rab11_1F** 5'-GACATTGCCAAGCATCTGAC-3', **Rab11_1R** 5'-GTTCTGGTCGGCATGGTC-3',

**Rab11_2F** 5'-AGCCACAGTTTGTCATGTGC-3', **Rab11_2R** 5'-TCTGATGATGGTGGTGGTGT-3' **Hrs_1F** 5'-AAGATGAACTCGCCCAACC-3', **Hrs_1R** 5'-GCAGTTCTTGACGATGCTCTC-3', **Hrs_2F** 5'-TCACTCCCAAGAATGCCTTT-3', **Hrs_2R** 5'-GAGGGAATAGCAGGAGGAGTG-3', **TSG101**_1F 5'-GACCTGCAGAGGTTCGTGTT-3', **TSG101_1R** 5'-CGGGAATAGTGCCCTGTATG-3', **TSG101_2F** 5'-CTTATATGCCTCAGCCTGGTG-3', **TSG101_2R** 5'-GCTGTGGGATAAGGCAGAAA-3', **Actin-F** 5'-CACCTGCACACCATCATCATTAT-3', **Actin_R** 5'-CACACAACATGCGCCCAA-3', **Tub_F** 5'-TCCAATCGCAACAAAAAATTCA-3', **Tub_R** 5'-TCGTTTTCGTATGCTTTTCAGTGT-3', **RP49_F** 5'-GACGCTTCAAGGGACAGTATCTG-3', **RP49_R** 5'-AAACGCGGTTCTGCATGAG-3'

**Statistical Analysis**

All statistical analysis was carried out in R[51]. Data were tested for normality using Shapiro-Wilk tests (data were logged for normality where required), and for homogeneity of variance using Bartlett tests.

**Models for treatment effects on gradient length**

For the Ptc reporter a Kruskal Wallis test of gradient length against treatments related to exovesicle production (Wildtype, *UAS-aSmase-RNAi*, *UAS-Vps22-RNAi*, UAS-*Vps24-RNAi, UAS-Ykt6-RNAi, UAS-CG31729 (P4ATPase)-RNAi*) (n=65) showed a significant effect of treatment ($Chi^2$=34.11, df=5 P<0.001). Pairwise Wilcoxon tests adjusted for multiple comparisons were used to test for differences between control and each treatment (Fig. 6 Ad). For the Ci reporter a Kruskal Wallis test of gradient length against treatments related to exovesicle production (Wildtype, *UAS-Hrs-RNAi*, *UAS-Vps22-RNAi*, UAS-*Vps4-RNAi, UAS-Anxb11-RNAi, UAS-TSG101-RNAi, UAS-Vps24-RNAi, UAS-*$\alpha$*Smase-RNAi*), (n=87) showed a significant effect of treatment ($Chi^2$=36.89, df=7 P<0.001). Pairwise Wilcoxon tests adjusted for multiple comparisons were used to test for differences between control and each treatment (Fig. 6Ah).

**Models for treatment effects on number of EVs released**

A Kruskal Wallis test of the number of Hh-GFP puncta released for the control (*UAS-Hh-GFP*) and ten EVs related treatments (*UAS-ALIX-RNAi, UAS-AnxB11-RNAi, UAS-CG31729 (P4ATPase)-RNAi, UAS-Rab11- RNAi, UAS-Hrs-RNAi, UAS-Vps4-RNAi, UAS-Flo2-RNAi, UAS-TSG10-RNAi, UAS-YKT6-RNAi, UAS-aSmase-RNAi*)(n=103) showed a significant effect of treatment ($Chi^2$=54.67, df=10 P<0.001). Pairwise Wilcoxon tests adjusted for multiple comparisons were used to test for significant differences between control and each treatment (Fig 6Bc).

A Kruskal Wallis test carried out for the number of $Ihog^{RFP}$ puncta released for the control (*UAS-Ihog-RFP*) and seven treatments related to exosome production (*UAS-Alix-RNAi, UAS-TSG101-RNAi, UAS-AnxB11-RNAi, UAS-Rab11-RNAi, UAS-Hrs-RNAi, UAS-Vps4-RNAi, UAS-Flo2-RNAi)* (n=76) showed a significant effect of treatment ($Chi^2$=31.18, df=7, P<0.001). Pairwise Wilcoxon tests adjusted for multiple comparisons were used to test for significant differences between control and each treatment (Fig 6Bd)..

**Models for treatment effect on endogenous levels of external Hh**

A paired t-test comparing the relative fluorescence (mean gray values) for WT tissue and for RNAi treated tissue (*UAS-TSG101-RNAi, UAS-Rab11-RNAi, UAS-Hrs-RNAi, UAS-Vps22-RNAi*) (n=56) showed a significant difference (t = 13.18, df = 55, P<0.001). The Ratio WT:*ap* was tested for difference between RNAi expressing wing discs and discs without RNAi treatment or Control, using Anova ($F_{4,51}$=7.79, P>0.001). Tukey's Honest significant difference tests were used to test for differences between control and each treatment (Fig 6Cc).

**Models for treatment effect on endogenous levels of total Hh**

Paired t-tests comparing the relative fluorescence (mean gray values) for WT tissue and for RNAi treated tissue (*UAS-TSG101-RNAi, UAS-Hrs-RNAi, UAS-AnxB11-RNAi, UAS-Flo2-RNAi, UAS-Vps22-RNAi,* and *UAS-CG31729-RNAi (P4-ATPase*) (n=49) showed non-significant differences,

except for the TSG101 (t = -5.19, df = 7, p<0.01) and Vps22 (t=-5.50, df=7, p<0.001) treatments. The Ratio WT:*ap* was tested for difference between RNAi expressing wing discs (*ap*) and discs without RNAi treatment or control (WT), using Anova ($F_{6,42}$ = 11.7, p<0.001). Tukey's Honest significant difference tests showed that the only significant differences with control were for TSG101 (p<0.05) and Vps22 (p<0.001) (Supplementary Fig. 4Cc).

**Models for treatment effects on target RNA levels**

Welch two sample T-tests comparing the normalized values for RNA expression for WT tissue and for each RNAi treated tissue (*UAS-TSG101-RNAi, UAS-Flo2-RNAi, UAS-Rab11-RNAi, UAS-Hrs-RNAi*) showed significant differences between RNAi expressing larvae and larvae without RNAi treatment or Control (Supplementary Fig. 4B). Values for each treatment are: TSG101 RNAi against Control (n=6) (t=3.63, df=3.6 p<0.05), Flo2 RNAi against Control (n=6) (t=9.19, df=2.5 p<0.005), Rab11 RNAi against Control (n=6) (t=18.2, df=2 p<0.005), HRS RNAi against Control (n=12) (t=4.08, df=8.3 p<0.005).

**Immunoelectron Microscopy**

Larvae were inverted in PBS and fixed in 2% (w/vol) paraformaldehyde (PFA) and 0.2% (w/vol) glutaraldehyde (GLA) or 4%PFA and 0.05% GLA in 0.2 M phosphate buffer (PB, pH 7.4) for 2 h at room temperature and kept in 1% (w/vol) PFA in PB at 4 °C. Subsequently, wing discs were dissected, embedded in 10% (w/vol) gelatine, and processed for cryosectioning. Discs were then cut orthogonal to the ventral/dorsal axis on an EM FCS cryo-ultramicrotome (Leica Microsystems) at -120 °C. For immunogold labelling, thawed 90-nm thick cryosections were incubated with rabbit anti-GFP (1:500, A-6455; Invitrogen, rabbit anti-Hh (1:150) (6), guinea pig anti-Disp (1:100) antibodies followed by protein A conjugated to 15-nm gold particles (EM Laboratory, Utrecht University, The Netherlands). Sections were stained with a mix of 1.8% methylcellulose and 0.4% uranyl acetate. For double labelling, anti-Disp[8] and anti-Hh[48] antibodies were detected with goat

anti-guinea pig IgG conjugated to 10-nm gold particles and goat anti-rabbit IgG conjugated to 15-nm gold particles (British Biocell), respectively.

For *ex vivo* anti-GFP labelling experiments, discs expressing Hh-GFP were labelled with 1:30 dilution anti rabbit anti-GFP polyclonal antibody (Life technologies (Molecular Probes)) as reported[46] and fixed with 4%PFA and 0.05% GL in 0.2 M PB (pH 7.4) for 2h at RT. Then, the discs were processed for cryosectioning as described before. Ultrathin (100 nm) thawed cryosections were incubated with an anti-rabbit Fab´ fragment conjugated to Alexa594 and 1.4-nm nanogold (Fluoronanogold, Nanoprobes, New York, USA), mounted with 50% glycerol and visualized with an inverted fluorescence microscope (DMI6000, Leica Microsystems, Wetzlar, Germany). For EM visualization, nanogold labelling was amplified by silver enhancement according to manufacturer's instructions (Nanoprobes). Sections were then stained with a mixture of methylcellulose and uranyl acetate and visualized with a JEOL JEM 1010 (Tokyo, Japan) electron microscope operating at 80 kV. Images were recorded with a 4k x 4k CMOS F416 camera from TVIPS (Gauting, Germany).

**Immunoprecipitation**

We modified a standard protocol for immunoprecipitation using Drosophila embryos[52]. Larvae expressing CD63-GFP, Ihog-RFP or co-expressing both under *tub*.Gal4 were collected and dry frozen in liquid Nitrogen. 50 frozen larvae for each genotype were homogenized in 1 ml/each of C Buffer (50mM HEPES [pH7.4], 50mM KCl, 1mM MgCl, 1mM EGTA, 0.1% Triton, Protease inhibitors cocktail [Roche] and 1mM PMSF). Extracts were initially clarified by centrifugation at 35,000 x *g* for 10 min, followed by two consecutive high-speed centrifugations at 35,000 RPM for 10 min and the second for 30 min. Clarified supernatant was transferred to fresh tubes between each spin. The supernatant was then incubated with GFP-Trap coupled to agarose beads (Chromoteck) for 1 hour at 4°C, followed by washing (5X) with C Buffer. Immunoprecipitated samples were resuspended in sample buffer with DTT and subjected to 1 D SDS-Page and

Western blotting. Blotted membranes were probed with appropriate antibodies, either to RFP (1:5000, Abcam) or GFP (1:1000, Sigma). After antibody stripping (Tris-HCL 0.5 M, pH 6.8, 2% SDS and β-mercaptoethanol 0.1 M, for 30 min at 60°C) membranes were probed with anti-Hh (rabbit antibody raised for this work 1:5000). Uncropped Western blots are shown in Supplementary Fig. 5 A-C.

**Cell culture**

*Drosophila* S2 cells stably-expressing full-length Hh fused to green fluorescent protein (S2::Hh-GFP) were generated using the multicistronic vector pAc5-STABLE2-Neo[53], and cultured in Schneider's medium supplemented with 10% FBS and 1% penicillin/streptomycin at 25°C. Cl8 cells were cultured in M3 medium containing 2.5% of FBS, 2.5% fly extract, 10 mg/ml of insulin and 1% penicillin/streptomycin. Transient transfections of Cl8 cells were performed using X-tremeGENE transfection reagent (Roche Applied Science) following manufacturer's instructions on 25 million (5 million/ml) cells and 6 μg of DNA per transfection experiment.

**Production and isolation of EVs**

Crude preparation of EVs from Hh-GFP transiently transfected Cl8 cells were obtained by collecting 5 ml of EV-depleted media and performing differential centrifugation at 2,000 x *g* and 100,000 x *g* of the supernatants after 48 h transfection period. The pellets containing crude EVs were resuspended. For EV production of S2::Hh-GFP and Cl8 cells, 400 million cells were cultured for 48-h and 96-h, respectively, in EV-depleted media (2.5 millions/ml), and exosomes-enriched EVs secreted into the medium were purified as previously described[54]; briefly, culture supernatant was collected and centrifuged at 2,000 *x g,* 4°C, for 10 min to remove cells. The resultant supernatant was subjected to filtration through 0.22 μm pore filters, followed by ultracentrifugation at 10,000 *x g* and 100,000 *x g* for 30 min and 60 min, 4°C, respectively. The resulting pellets were washed with PBS and again submitted to ultracentrifugation at 100,000 *x g*,

4°C, for 60 min. Final pellets were suspended in PBS and stored at - 80ºC.

**Western blot analysis**

A small portion (1/350th) of the supernatants obtained after 2,000 x *g* and 100,000 x *g,* and 1/5th of the crude EVs preparations or of the fractions from the sucrose gradient were analysed by Western-blotting. Extracts from larvae stage 3 (L3) were prepared as described[7]. SDS-sample buffer was added to the samples and incubated for 5 min at 37ºC, 65ºC and 95ºC and separated on 4-12% pre-casted acrylamide gels (Invitrogen, Carlsbad, CA) under non-reducing conditions. Gels were transferred to PVDF membranes and blocked (5% milk and 0.05% Tween-20 in PBS) for antibody incubation. Chemoluminescent detection of proteins was performed using ECL Prime (Amersham) or Clarity Western ECL substrate (Biorad). Monoclonal antibodies were purchased from the vendors indicated: anti-GFP (clones 7.1 and 13.1) from Roche, anti-GFP (clone GFP-20) for co-immunoprecipitation experiments from Sigma, anti-RFP (ab62341) from Abcam, anti-Hsp70 (BRM-22) from Santa Cruz Biotech. Inc (Santa Cruz, CA), anti-TSG101 (4A10) from Abcam, anti-Rab11 (clone 47) and anti-ubiquitin (clone 6C1.17) from BD Biosciences (Mountain View, CA), anti-ApoLII[55] and anti-Syntaxin (8C3) from Developmental Studies Hybridoma Bank (Iowa City, IA). Rabbit polyclonal anti-Hh and anti-Ihog were obtained using the Polyclonal Genomic Antibody TechnologyTM (sdix)[56]. For the anti-Hh production, the immunogen region used comprised the DmHh amino-acids region 80-256; as for the anti-Ihog the DmIhog amino-acid region 248-488 was used. Horseradish peroxidase (HRP)-conjugated secondary antibody was from GE-Healthcare (Buckinghamshire, UK). Uncropped Western blots are shown in Supplementary Fig. 5 D-I.

**Fractionation of EVs on continuous sucrose gradient**

A continuous 0.25–2 M sucrose gradient in 20 mM HEPES (pH 7.4) was performed as described in[57]. Briefly, EVs were put on top of the continuous sucrose gradient and submitted to ultracentrifugation for 16 h at 210 000 × *g*, 4°C, in a SW40Ti swinging-bucket rotor. By using an

auto densi-flow density gradient fractionator (Labconco, Kansas City, MO, USA), one millilitre fractions were collected from top to bottom and 20 µL of each fraction were reserved for measurement of the refractive index to density determination. Each fraction was diluted with 2 mL of 20 mM HEPES (pH 7.4) and ultra-centrifuged for 1 h at 100 000 × *g*, 4°C, in a TLA-110 rotor. Supernatants were aspirated and pellets were suspended in 25 µL PBS and stored at −80°C.

**Gene silencing in *Drosophila* cultured Cl8 cells**

nSMase, TSG101 and Rab27 dsRNAs were synthesized following the protocol used at the *Drosophila* RNAi Screening Centre (DRSC) in Boston. Briefly, DNA templates containing T7 promoters sequence on both ends were obtained from the DRSC and were amplified by PCR. These PCR products were used for the *in vitro* transcription (IVT) reaction, which was carried out for 16 h at 37ºC using the T7 Megascript kit from Ambion. After DNaseI (Ambion) digestion to remove the template DNA, the dsRNAs were purified using RNAeasy columns (QIAGEN). Both PCR-amplified DNA and purified dsRNA products were assessed by gel electrophoreses and absorbance measurements of the yield. Cl8 cells were seeded in six-well plates at $2\times10^6$ per well in 0.5 mL of FBS-free medium and 7.5 $\mu$ g of dsRNA were added and incubated for 1h, adding then 1.5 mL of EV-depleted medium. After 48 h of incubation a new dose of dsRNA was added and after another 48h of incubation the supernatants were collected and centrifuged at 2 000 *x g* for 10 min to remove cells, then centrifuged at 100 000 × *g* for 1 h, 4°C, in a TLA-110 rotor. The resulting pellets were suspended in 25 µL of PBS and stored at −80°C for subsequent analysis by Western blotting.

**Luciferase activity assay of Hh EVs on cultured *Drosophila* cells**

Cl8 cells were transfected with ptc Δ 136-GL3 Firefly responsible reporter [58]. After 24 h, cells were lifted and seeded into 96-wells plate, and 8-hours later incubated with 0.2 ng/ul of Shh recombinant protein (Sigma) or 1/4th of the crude EVs. After 24 h of treatment, Firefly luciferase

levels were measured using the Dual-Glo Luciferase Assay System (Promega) and the ratio to the control (no EVs added) was calculated to give the Hh signalling activity. This was tested in triplicate and significant differences were tested by a t-student test.


## ACKNOWLEDGEMENTS

We are very grateful to MC Rodríguez-Navas for technical assistance, to T. Tabata for the α-Hh antibody for Immune-EM studies, B. Holmgren for the α-Ci, S. Eaton for the UAS-CD63-GFP fly line and R. Wilson who assisted with statistical analysis, and the BDSC and VDRC for stocks. We also thank the Genomic and the Confocal microscopy facilities of the Centro de Biología Molecular "Severo Ochoa," for skilful technical assistance. Work was supported by grants from the Consolidation Program (CSD2007-008-25120) to RB and IG, by grants BFU2011-25987 to IG, BFU2011-25986 to RB, and BFU2009-08085 to GA from the Spanish MICINN, by Marie Curie FP7 (ITN 238186) and by an institutional grant to the CBMSO from the Fundación Areces to IG, and by the Departments of Education and Industry of the Basque Government (PI2009-16 and PI2012/42), and the Bizkaia County to RB. ACG and JROF were financially supported by a Marie Curie ITN FP7 contracts, IS was financially supported by a FPI fellowship of the Spanish MICINN, AC by fellowships awarded by the JAE-CSIC program (2008-2011), GA by a senior researcher AMAROUTO program of the Comunidad Autónoma de Madrid.


## AUTHOR CONTRIBUTIONS

- Ana-Citlali Gradilla, performed Drosophila silencing experiments, the IP assays, the imaging and statistical analysis and wrote the manuscript.- Esperanza González, Laura González-Mendez, Vanessa Sánchez[1] James D. Sutherland, -Monika González, Rosa Barrio, did the in vitro tissue culture experiments.

- Irene Seijo performed silencing experiments, immunostaining and the confocal images of the Drosophila imaginal discs as well as quantitative RT-PCR experiments.

- Ainhoa Callejo, Carmen Ibáñez performed immunostaining and the confocal images of the Drosophila imaginal discs.

- German Andrés designed and Milagros Guerra performed the immune-electromicroscopy experiment.

- Marcus Bischoff performed the in vivo movies to visualize exosomes in the Drosophila adult abdomen.

- João Ramalho Ortigão-Farias collaborated in obtaining and characterised the anti Hh and anti Ihog polyclonal antibodies.

- Juan M. Falcón-Pérez designed the in vitro tissue culture experiments.

- Isabel Guerrero designed the experiments and wrote the manuscript.

**COMPETING FINANCIAL INTERESTS**

No competing financial interests

**FIGURE LEGENDS.**

**Figure1: Hh and key signalling components are present in EVs and cytonemes.** A) Schematic representation of a cross-section of the wing disc showing the expression of Hh [21] in both epithelia; Disc proper (DP) and peripodial membrane [59]. B) Transverse section of a *hh*.Gal4>UAS.Hh$^{GFP}$ wing disc which has been *ex-vivo* stained with anti-GFP antibody for one hour at low temperature to avoid Hh$^{GFP}$ internalization. Note the colocalization of Hh$^{GFP21}$ and externalized GFP (red) mainly at the basolateral part of the disc epithelium (bottom of image). C) Confocal sections of a similar *hh*.Gal4>UAS.Hh$^{GFP}$ wing disc *ex-vivo* stained with anti-GFP antibody. Note that the colocalization of green [60] and red (externalized Hh) is increased in more basolateral sections. The internalized Hh$^{GFP}$ at the A compartment is in green (white arrow heads). Note also that in the most basal section Hh puncta appear to be aligned in a 'beads on a

602 string' arrangement, suggesting they associate to cytonemes (see also [6]). D) *Ex-vivo* staining
603 using an anti-GFP antibody in a UAS.Hh$^{GFP}$/UAS.Ihog$^{RFP}$; *hh.Gal4*/tubGal80$^{ts}$ wing disc after 24
604 hours at the restrictive temperature. Note the colocalization between Hh and Ihog (arrow heads)
605 in the A compartment and also the presence of externalized Hh at the cellular extensions marked
606 by the Ihog protein. E) Dlp expression in a tubGal80$^{ts}$; UAS.Ihog$^{YFP}$/*hh.Gal4* wing disc for 24
607 hours. e) Insets in E showing the colocalization of puncta of Ihog and Dlp (arrow heads) in the A
608 compartment. F) Ectopic expression of UAS-Ihog$^{YFP}$ and UAS-Disp using the *hhGal4*; tubGal80$^{ts}$
609 system for 24 hours. f) Insets in F show the colocalization of puncta of both proteins (arrow
610 heads) in the A compartment. G) *Ex-vivo* staining using an anti-Disp antibody in a UAS-
611 Disp/UAS-iHog$^{CFP}$; *hhGal4*/tubGal80$^{ts}$ wing disc after 24 hours at the restrictive temperature. Note
612 the colocalization of Disp, Dlp and Ihog in the A compartment (arrow heads) (insets g). Bars,10
613 μm.

614 **Figure 2: Hh and Ihog can complex with the exosome marker CD63 *in vivo*.** A) Lateral view
615 of a reconstructed z –stack of confocal images from a wing disc expressing the exosome marker
616 UAS.CD63$^{GFP}$ and UAS.Ihog$^{RFP}$ under the control of *hh.Gal4*/tubG80$^{ts}$ after 24 hours at the
617 restrictive temperature and immuno-labeled for Hh. Note the colocalization of Ihog$^{RFP}$ (red) and
618 Hh (grey) with the marker CD63$^{GFP21}$ (arrow heads). Bar 20 μm. B) Live imaging of *Drosophila*
619 abdomen shows CD63$^{GFP}$ labelled puncta that co-localizes with puncta also labelled by Ihog$^{RFP}$
620 (arrow heads) and that move along the cytoneme (See also Supplementary Movie 3). Bar 10 μm.
621 C-E) Western Blots showing co-immunoprecipation of CD63$^{GFP}$, IhogRFP and endogenous Hh
622 after a GFP-Trap pull down (Chromoteck) from a High Speed Supernatant (HSS) of homogenized
623 larvae expressing CD63$^{GFP}$ as control and larvae co-expressing CD63$^{GFP}$ and Ihog$^{RFP}$ as
624 expermiental. (C) Immunoprecipitation of CD63$^{GFP}$ shown for both, the IP control and the
625 experimental IP (arrowhead). (D') Co-immunoprecipitation of Ihog$^{RFP}$ revealed by anti-RFP in the
626 experimental IP (arrow) and not present in the IP control. D'') Co-immunoprecipitation of

endogenous Hh revealed (after membrane antibody stripping) by anti-Hh in the experimental IP (asterisk) and not present in the IP control, probably due to an enrichment effect of the co-expression of Ihog$^{RFP}$ and CD63$^{GFP}$.

**Figure 3. Punctate structures move along cytonemes *in vivo*.** (**A,B**) CD63$^{GFP}$ labels punctate structures that move along cytonemes. Cells of the P compartment are labelled with hh.*Gal4>UAS.CD63$^{GFP}$*. (**A**) Individual frames taken from Supplementary Movie 4. Black arrows indicate puncta. Fluorescence is depicted using an inverted grey lookup table[61]. (**B**) Individual frames taken from Supplementary Movie 5. Arrowheads indicate puncta. Fluorescence is depicted using a grey LUT (left) and a HiLo LUT (right), which highlights the brightest pixels in red. (**C**) Cytonemes labelled with CD4-Tomato show 'buckling' and 'swelling' (C). These structures might be related to the shedding of vesicles, which we could observe occasionally (see D). Individual frames taken from Supplementary Movie 6. Cells of the P compartment are labelled with hh.*Gal4 >UAS.CD4-Tomato*. Fluorescence is depicted using an inverted grey lookup table.. (**D**) Occasionally, we observe punctate structures shedding from the cytonemes. Individual frames taken from Supplementary Movie 7. Cytonemes reaching into the A compartment are labelled with *hh.Gal4>UAS.Ihog$^{RFP}$* and coloured with a fire look-up table. Left panel: Overview. Right panels: Time sequence of detail indicated in the overview. Note punctate structures, which are located along the cytonemes. One punctum (white arrows) is budding (cyan arrowheads) and finally shedding from the cytoneme (orange arrowhead).

**Figure 4: Ultrastructural localization of Hh in imaginal discs.** Correlative light-electron microscopy of wing discs expressing Hh-GFP. Discs were labelled *ex vivo* with a rabbit anti-GFP antibody and then fixed and processed for cryosectioning. Ultrathin sections, cut orthogonally to the V/D axis, were incubated with a fluorescent (Alexa594) 1.4-nm nanogold-conjugated anti-rabbit Fab´ probe. Labelled cryosections were first imaged at the fluorescence microscope (A1) and then at the transmission electron microscope after silver enhancement of the nanogold signal

(A2-F1). At the light microscopy level (A1) fluorescent labelling is detected at apical areas and at basolateral regions of the P compartment. At the EM level, apical immunogold labelling (B and B1 shows the area delimited by a red box/square/rectangle in A) decorated microvilli membranes (arrows in B1) whereas basolateral signal (panels C1-C3 shows EM images of the area delimited by a blue square in A while D-F shows details of a different disc) is mainly associated with discrete extents of the plasma membrane (arrows in C1, C3 and D) that frequently coincide with cell-to-cell contacts (arrows in D). Also, immunogold labelling is detected in clusters of extracellular vesicle-like structures (arrowheads in panels C1.1, C3, D1, E1, E2 and F1), some of which are associated with cell protrusions (insets in C1 (C1.1) and E (E1)). A and P compartments as well as apical (Ap) and basolateral (Bs) regions are indicated in panels A1 and A2. To help the interpretation, apical and basolateral extracellular spaces are depicted in red (B) and blue (C1, C3, D, E and F), respectively. Panels A to C3 correspond to the same wing disc whereas panels D to F1 correspond to a different specimen. Abbreviations: LD (lipid droplet). Bars: 25 µm (A1 and A2), 5 µm (C), 500 nm (B, C2, D, E and F), 200 nm (B1, C1, C3, D1, E1 and E2) and 100 nm (C1.1 and F1).

**Figure 5: Hedgehog protein is associated to EVs with features of exosomes.** A) A representative Western blotting of supernatants (SN1500 and SN45) and EVs obtained from 5 ml of media from mock- (control) or Hh-GFP- transfected Cl8 cells. Similar volume of supernatants (1/350 of the total) and 1/5th of the EVs were applied to the gel. Antibodies against indicated proteins were used as described in *Materials and Methods.* Antibody against Hh showed that Hh is found in EVs, although the Hh-associated to EVs represents less than 10% of the total secreted forms (n=3) B) EVs from Hh-GFP transfected cells were fractionated by continuous sucrose density gradient and equal amounts (1/5th) of the resulting fractions analysed by Western blotting. Specific antibodies show the presence of Hh and protein markers of exosomes (Ubiquitinated proteins, Hsp70, TSG101 and Rab11) mapping at similar densities. ApoLII was

677 also tested in the gradient, showing a different pattern along the gradient. C) Western blot
678 analysis of Hedgehog protein in EVs obtained from untransfected Cl8 cells and extract from
679 larvae stage 3 (L3). D) Luciferase activity in Cl8 cells transfected with ptc Δ 136-GL3 Firefly
680 responsible reporter and incubated without (Control) or with EVs obtained from Cl8 cells. Shh
681 recombinant protein was used as positive inducer. Mean ± SD of three replicates is shown.
682 Significance level (t-student test) **P<0.01.

683 **Figure 6: Hh signalling and release in mutant conditions for exosome production genes.**
684 A) Hh signalling in wing discs expressing RNAi treatments in the P compartment (b-d, f-h) and
685 control (a,e), visualized in the A compartment using the Ptc-promotor-Trap::GFP reporter (a-d)
686 and immunolabelling for the long range target Ci (e-h). Detail shown at the bottom and anterior is
687 to the left. Note in RNAi wing discs (b-d, f-h), gradients are shorter than in controls (a,e). (d,h)
688 Box plot comparing gradient length expressed as a proportion of wing pouch length, between
689 control discs and treatments for each reporter. B) Quantification of the number of $Hh^{GFP}$ (a-c) or
690 $Ihog^{RFP}$ (d) released punctate structures. Reconstruction in Z (lateral view) of wing discs
691 expressing $Hh^{GFP\ 21}$ (a) or coexpressing $Hh^{GFP}$ and RNAi for AnxB11 (b) under the control of
692 *hh.Gal4* and immunostained for the transcription target Ptc (red), note punctate structures in the
693 A compartment, decrease after RNai treatment. (c) Boxplot comparing the number of $Hh^{GFP}$
694 puncta released for the control (*UAS.*$Hh^{GFP}$) and ten exosome related treatments. Note the
695 reduction in the number of puncta. (d) Boxplot comparing the number of $Ihog^{RFP}$ puncta (anterior
696 compartment) for the control (*UAS.*$Ihog^{RFP}$) and seven treatments related to exosome production.
697 Note the reduction in the number of puncta. C) Endogenous externalized Hh levels decrease in
698 mutant conditions for exosome production genes. *Ex-vivo* staining for Hh in wild type discs (a) or
699 in wing disc expressing RNAi for TSG010 (b) driven by *ap.Gal4* with a dorsal expression domain
700 (marked by GFP), leaving the ventral domain in Wild Type conditions as an internal control. Note
701 the decrease in fluorescence after treatment (a,b). (c) Boxplot showing the ratio between relative

intensity of the mean grey value in the dorsal (RNAi treated) versus the ventral compartment (Wild type). The ratio is close to 1 in control while ratio for all RNAi cases is greater than 1 due to a decrease in the levels of external Hh in treated cells. Significance levels for pairwise tests (Tukey HSD or Wilcoxon, depending on Normality of data): *** P<0.001, ** P<0.01, *P<0.05, + P<0.1. Bars,10 μm.

## REFERENCES


1 Briscoe, J. & Therond, P. P. The mechanisms of Hedgehog signalling and its roles in development and disease. *Nat Rev Mol Cell Biol* **14**, 416-429, (2013).

2 Porter, J. A., Young, K. E. & Beachy, P. A. Cholesterol modification of hedgehog signaling proteins in animal development. *Science* **274**, 255-259 (1996).

3 Pepinsky, R. B. *et al.* Identification of a palmitic acid-modified form of human Sonic hedgehog. *J Biol Chem* **273**, 14037-14045 (1998).

4 Callejo, A., Torroja, C., Quijada, L. & Guerrero, I. Hedgehog lipid modifications are required for Hedgehog stabilization in the extracellular matrix. *Development* **133**, 471-483, (2006).

5 Ramirez-Weber, F. A. & Kornberg, T. B. Cytonemes: cellular processes that project to the principal signaling center in Drosophila imaginal discs. *Cell* **97**, 599-607 (1999).

6 Bischoff M., *et al.* Cytonemes are required for the establishment of a normal Hedgehog morphogen gradient in Drosophila epithelia. *Nature Cell Biology* (2013).

7 Bilioni, A. *et al.* Balancing Hedgehog, a retention and release equilibrium given by Dally, Ihog, Boi and shifted/DmWif. *Dev Biol* **376**, 198-212, (2013).

8 Callejo, A. *et al.* Dispatched mediates Hedgehog basolateral release to form the long-range morphogenetic gradient in the Drosophila wing disk epithelium. *Proceedings of the National Academy of Sciences of the United States of America* **108**, 12591-12598, (2011).

9 Sanders, T. A., Llagostera, E. & Barna, M. Specialized filopodia direct long-range transport of SHH during vertebrate tissue patterning. *Nature* **497**, 628-632,(2013).

10 Struhl, G., Barbash, D. A. & Lawrence, P. A. Hedgehog organises the pattern and polarity of epidermal cells in the Drosophila abdomen. *Development* **124**, 2143-2154 (1997).

11 Burke, R. *et al.* Dispatched, a novel sterol-sensing domain protein dedicated to the release of cholesterol-modified hedgehog from signaling cells. *Cell* **99**, 803-815 (1999).

12 Panakova, D., Sprong, H., Marois, E., Thiele, C. & Eaton, S. Lipoprotein particles are required for Hedgehog and Wingless signalling. *Nature* **435**, 58-65 (2005).

13 Simons, M. & Raposo, G. Exosomes--vesicular carriers for intercellular communication. *Curr Opin Cell Biol* **21**, 575-581, (2009).

14 Subra, C., Laulagnier, K., Perret, B. & Record, M. Exosome lipidomics unravels lipid sorting at the level of multivesicular bodies. *Biochimie* **89**, 205-212,(2007).
15 Simpson, R. J., Jensen, S. S. & Lim, J. W. Proteomic profiling of exosomes: current perspectives. *Proteomics* **8**, 4083-4099, (2008).
16 Savina, A., Vidal, M. & Colombo, M. I. The exosome pathway in K562 cells is regulated by Rab11. *J Cell Sci* **115**, 2505-2515 (2002).
17 Vidal, M. J. & Stahl, P. D. The small GTP-binding proteins Rab4 and ARF are associated with released exosomes during reticulocyte maturation. *Eur J Cell Biol* **60**, 261-267 (1993).
18 Kalra, H. *et al.* Vesiclepedia: a compendium for extracellular vesicles with continuous community annotation. *PLoS biology* **10**, e1001450, doi:10.1371/journal.pbio.1001450 (2012).
19 Palm, W. *et al.* Secretion and signaling activities of lipoprotein-associated hedgehog and non-sterol-modified hedgehog in flies and mammals. *PLoS biology* **11**, e1001505, doi:10.1371/journal.pbio.1001505 (2013).
20 van Niel, G. *et al.* The tetraspanin CD63 regulates ESCRT-independent and -dependent endosomal sorting during melanogenesis. *Dev Cell* **21**, 708-721,(2011).
21 Beckett, K. *et al.* Drosophila S2 cells secrete wingless on exosome-like vesicles but the wingless gradient forms independently of exosomes. *Traffic* **14**, 82-96, doi:10.1111/tra.12016 (2013).
22 Koles, K. *et al.* Mechanism of evenness interrupted (Evi)-exosome release at synaptic boutons. *J Biol Chem* **287**, 16820-16834, (2012).
23 Trajkovic, K. *et al.* Ceramide triggers budding of exosome vesicles into multivesicular endosomes. *Science* **319**, 1244-1247, (2008).
24 Wehman, A. M., Poggioli, C., Schweinsberg, P., Grant, B. D. & Nance, J. The P4-ATPase TAT-5 inhibits the budding of extracellular vesicles in C. elegans embryos. *Curr Biol* **21**, 1951-1959, (2011).
25 Gross, J. C., Chaudhary, V., Bartscherer, K. & Boutros, M. Active Wnt proteins are secreted on exosomes. *Nat Cell Biol* **14**, 1036-1045, (2012).
26 Colombo, M. *et al.* Analysis of ESCRT functions in exosome biogenesis, composition and secretion highlights the heterogeneity of extracellular vesicles. *J Cell Sci* **126**, 5553-5565, (2013).
27 Koppen, T. *et al.* Proteomics analyses of microvesicles released by Drosophila Kc167 and S2 cells. *Proteomics* **11**, 4397-4410, (2011).
28 Thery, C. *et al.* Proteomic analysis of dendritic cell-derived exosomes: a secreted subcellular compartment distinct from apoptotic vesicles. *Journal of immunology* **166**, 7309-7318 (2001).
29 de Gassart, A., Geminard, C., Fevrier, B., Raposo, G. & Vidal, M. Lipid raft-associated protein sorting in exosomes. *Blood* **102**, 4336-4344, (2003).
30 Muralidharan-Chari, V. *et al.* ARF6-regulated shedding of tumor cell-derived plasma membrane microvesicles. *Curr Biol* **19**, 1875-1885, (2009).
31 Cocucci, E., Racchetti, G., Podini, P. & Meldolesi, J. Enlargeosome traffic: exocytosis triggered by various signals is followed by endocytosis, membrane shedding or both. *Traffic* **8**, 742-757, (2007).
32 Del Conde, I., Shrimpton, C. N., Thiagarajan, P. & Lopez, J. A. Tissue-factor-bearing microvesicles arise from lipid rafts and fuse with activated platelets to initiate coagulation. *Blood* **106**, 1604-1611, (2005).
33 Jimenez, A. J. *et al.* ESCRT machinery is required for plasma membrane repair. *Science* **343**, 1247136 (2014).

34 Langelier, C. *et al.* Human ESCRT-II complex and its role in human immunodeficiency virus type 1 release. *Journal of virology* **80**, 9465-9480, (2006).

35 Teis, D., Saksena, S., Judson, B. L. & Emr, S. D. ESCRT-II coordinates the assembly of ESCRT-III filaments for cargo sorting and multivesicular body vesicle formation. *The EMBO journal* **29**, 871-883, (2010).

36 Henne, W. M., Stenmark, H. & Emr, S. D. Molecular mechanisms of the membrane sculpting ESCRT pathway. *Cold Spring Harbor perspectives in biology* **5**, (2013).

37 Greco, V., Hannus, M. & Eaton, S. Argosomes: a potential vehicle for the spread of morphogens through epithelia. *Cell* **106**, 633-645 (2001).

38 Tanaka, Y., Okada, Y. & Hirokawa, N. FGF-induced vesicular release of Sonic hedgehog and retinoic acid in leftward nodal flow is critical for left-right determination. *Nature* **435**, 172-177, (2005).

39 Liegeois, S., Benedetto, A., Garnier, J. M., Schwab, Y. & Labouesse, M. The V0-ATPase mediates apical secretion of exosomes containing Hedgehog-related proteins in Caenorhabditis elegans. *The Journal of cell biology* **173**, 949-961 (2006).

40 Luz, M. *et al.* Dynamic association with donor cell filopodia and lipid-modification are essential features of Wnt8a during patterning of the zebrafish neuroectoderm. *PloS one* **9**, e84922, doi:10.1371/journal.pone.0084922 (2014).

41 Eugster, C., Panakova, D., Mahmoud, A. & Eaton, S. Lipoprotein-heparan sulfate interactions in the Hh pathway. *Dev Cell* **13**, 57-71 (2007).

42 Zeng, X. *et al.* A freely diffusible form of Sonic hedgehog mediates long-range signalling. *Nature* **411**, 716-720 (2001).

43 Hinz, U., Giebel, B. & Campos-Ortega, J. A. The basic-helix-loop-helix domain of Drosophila lethal of scute protein is sufficient for proneural function and activates neurogenic genes. *Cell* **76**, 77-87, (1994).

44 Tanimoto, H., Itoh, S., ten Dijke, P. & Tabata, T. Hedgehog creates a gradient of DPP activity in Drosophila wing imaginal discs. *Mol Cell* **5**, 59-71, (2000).

45 Calleja, M., Moreno, E., Pelaz, S. & Morata, G. Visualization of gene expression in living adult Drosophila. *Science* **274**, 252-255 (1996).

46 Torroja, C., Gorfinkiel, N. & Guerrero, I. Patched controls the Hedgehog gradient by endocytosis in a dynamin-dependent manner, but this internalization does not play a major role in signal transduction. *Development* **131**, 2395-2408 (2004).

47 Han, C., Jan, L. Y. & Jan, Y. N. Enhancer-driven membrane markers for analysis of nonautonomous mechanisms reveal neuron-glia interactions in Drosophila. *Proceedings of the National Academy of Sciences of the United States of America* **108**, 9673-9678, (2011).

48 Capdevila, J. & Guerrero, I. Targeted expression of the signaling molecule decapentaplegic induces pattern duplications and growth alterations in Drosophila wings. *EMBO J* **13**, 4459-4468 (1994).

49 Takei, Y., Ozawa, Y., Sato, M., Watanabe, A. & Tabata, T. Three Drosophila EXT genes shape morphogen gradients through synthesis of heparan sulfate proteoglycans. *Development* **131**, 73-82 (2004).

50 Motzny, C. K. & Holmgren, R. The Drosophila cubitus interruptus protein and its role in the wingless and hedgehog signal transduction pathways. *Mechanisms of development* **52**, 137-150 (1995).

51 Crawley, M. J. *The R Book*. (John Wiley & Sons, 2007).

52 Hughes, J. R. *et al.* A microtubule interactome: complexes with roles in cell cycle and mitosis. *PLoS biology* **6**, e98, doi:10.1371/journal.pbio.0060098 (2008).
53 Gonzalez, M. *et al.* Generation of stable Drosophila cell lines using multicistronic vectors. *Sci Rep* **1**, 75, (2011).
54 Conde-Vancells, J. *et al.* Characterization and comprehensive proteome profiling of exosomes secreted by hepatocytes. *J Proteome Res* **7**, 5157-5166 (2008).
55 Kutty, R. K. *et al.* Molecular characterization and developmental expression of a retinoid- and fatty acid-binding glycoprotein from Drosophila. A putative lipophorin. *J Biol Chem* **271**, 20641-20649 (1996).
56 Chambers, R. S. & Johnston, S. A. High-level generation of polyclonal antibodies by genetic immunization. *Nat Biotechnol* **21**, 1088-1092, 2003).
57 Thery, C., Amigorena, S., Raposo, G. & Clayton, A. Isolation and characterization of exosomes from cell culture supernatants and biological fluids. *Curr Protoc Cell Biol* **Chapter 3**, Unit 3 22, (2006).
58 Nybakken, K., Vokes, S. A., Lin, T. Y., McMahon, A. P. & Perrimon, N. A genome-wide RNA interference screen in Drosophila melanogaster cells for new components of the Hh signaling pathway. *Nat Genet* **37**, 1323-1332, (2005).
59 R: A lenguage and Environment for Statistical Computing (R Foundation for Statistical Computing, Vienna, Austria, 2011).
60 Chhabra, E. S. & Higgs, H. N. The many faces of actin: matching assembly factors with cellular structures. *Nat Cell Biol* **9**, 1110-1121, (2007).
61 Grigliatti, T. A., Hall, L., Rosenbluth, R. & Suzuki, D. T. Temperature-sensitive mutations in Drosophila melanogaster. XIV. A selection of immobile adults. *Mol Gen Genet* **120**, 107-114 (1973).

# Figure 1

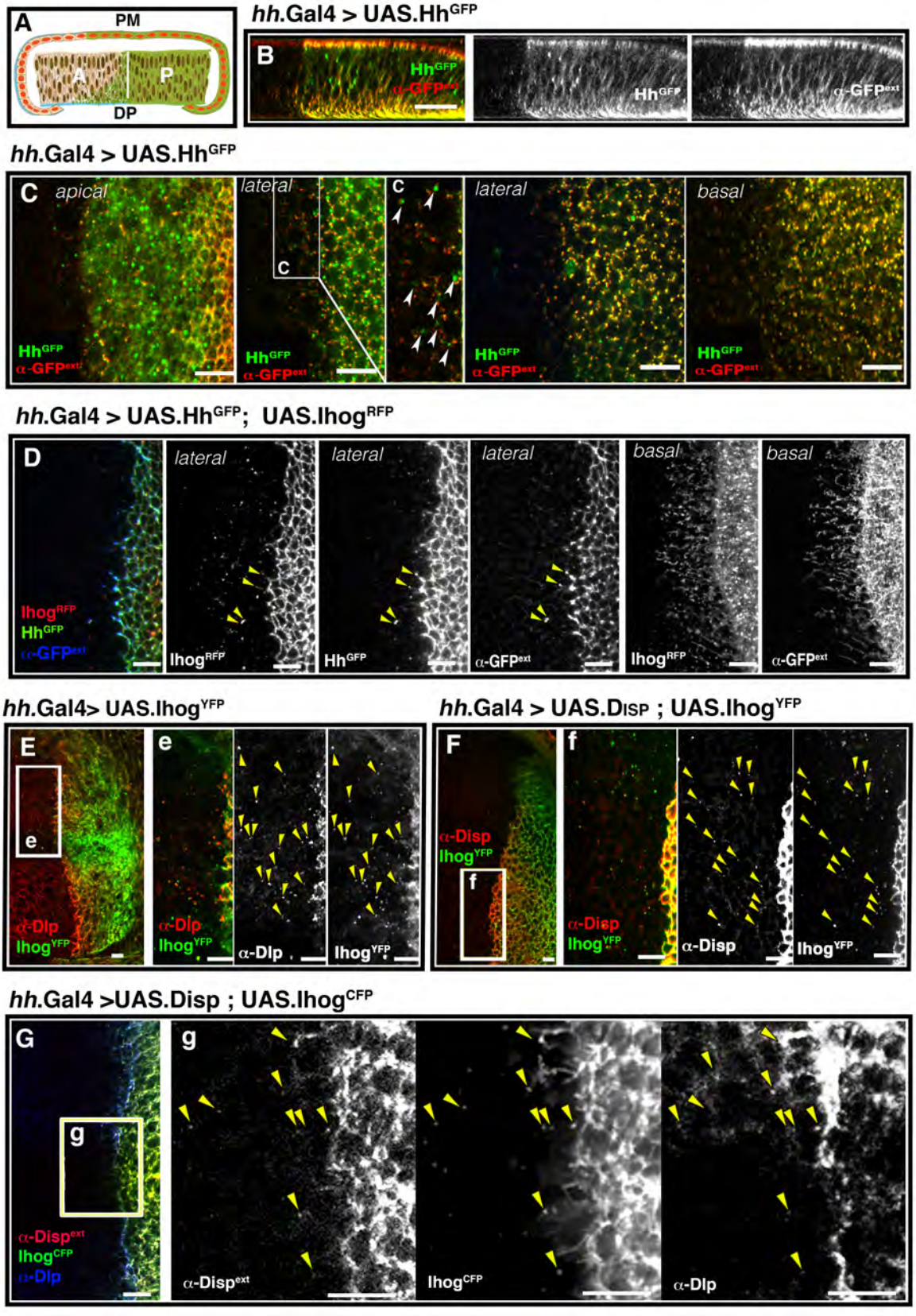
A
PM
A
P
DP
hh.Gal4 > UAS.Hh^GFP
B
Hh^GFP
α-GFP^ext
Hh^GFP
α-GFP^ext
hh.Gal4 > UAS.Hh^GFP
C
apical
lateral
c
c
lateral
basal
Hh^GFP
α-GFP^ext
hh.Gal4 > UAS.Hh^GFP; UAS.Ihog^RFP
D
lateral
lateral
lateral
basal
basal
Ihog^RFP
Hh^GFP
α-GFP^ext
Ihog^RFP
Hh^GFP
α-GFP^ext
Ihog^RFP
α-GFP^ext
hh.Gal4> UAS.Ihog^YFP
E
e
e
α-Dlp
Ihog^YFP
α-Dlp
Ihog^YFP
α-Dlp
Ihog^YFP
hh.Gal4 > UAS.Disp ; UAS.Ihog^YFP
F
f
α-Disp
Ihog^YFP
f
α-Disp
Ihog^YFP
α-Disp
Ihog^YFP
hh.Gal4 >UAS.Disp ; UAS.Ihog^CFP
G
g
α-Disp^ext
Ihog^CFP
α-Dlp
g
α-Disp^ext
Ihog^CFP
α-Dlp

# Figure 2

***hh*.Gal4 > UAS.Ihog$^{RFP}$; UAS.CD63$^{GFP}$**

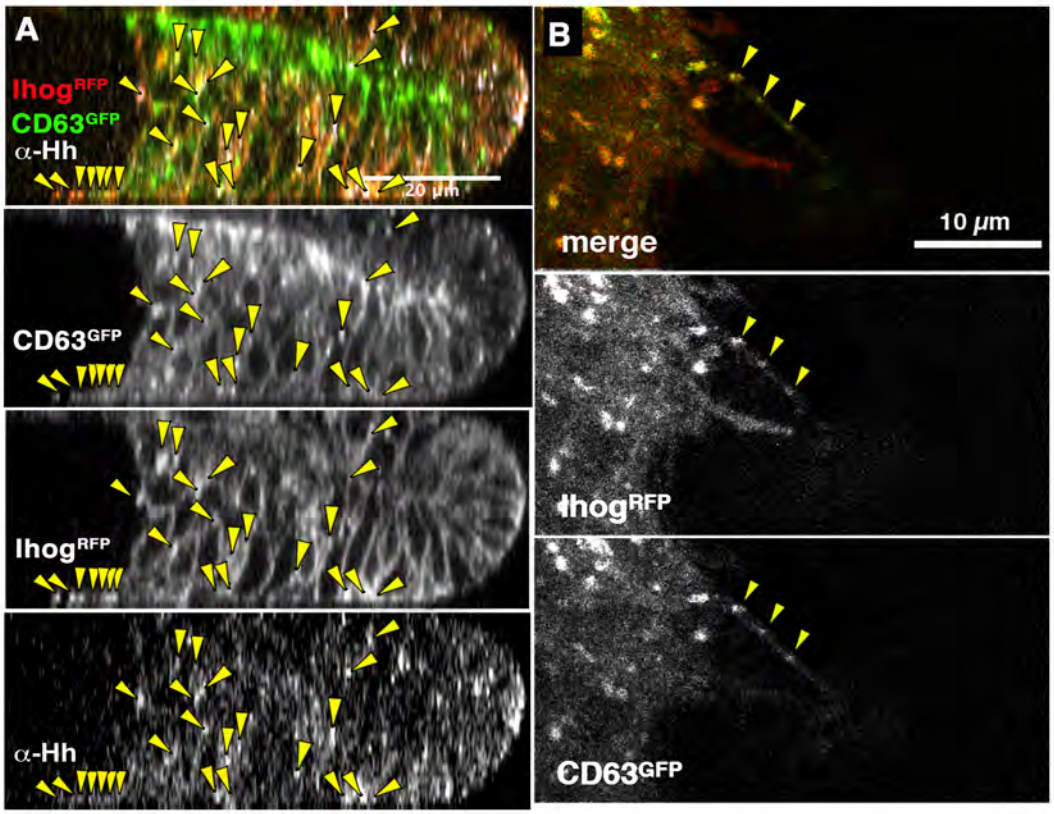


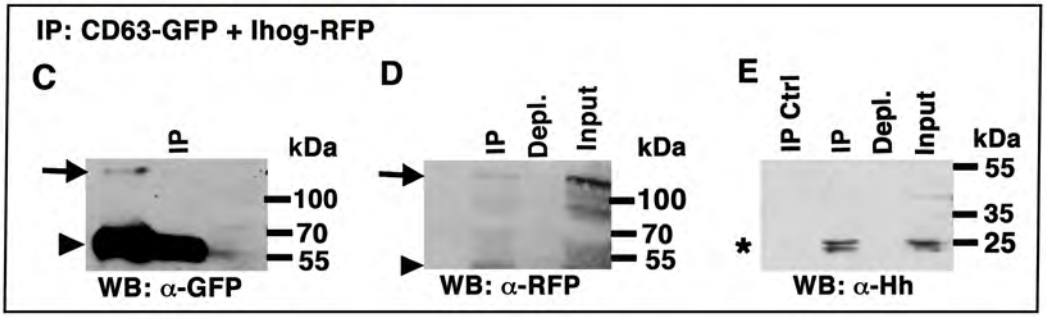

# Figure 3

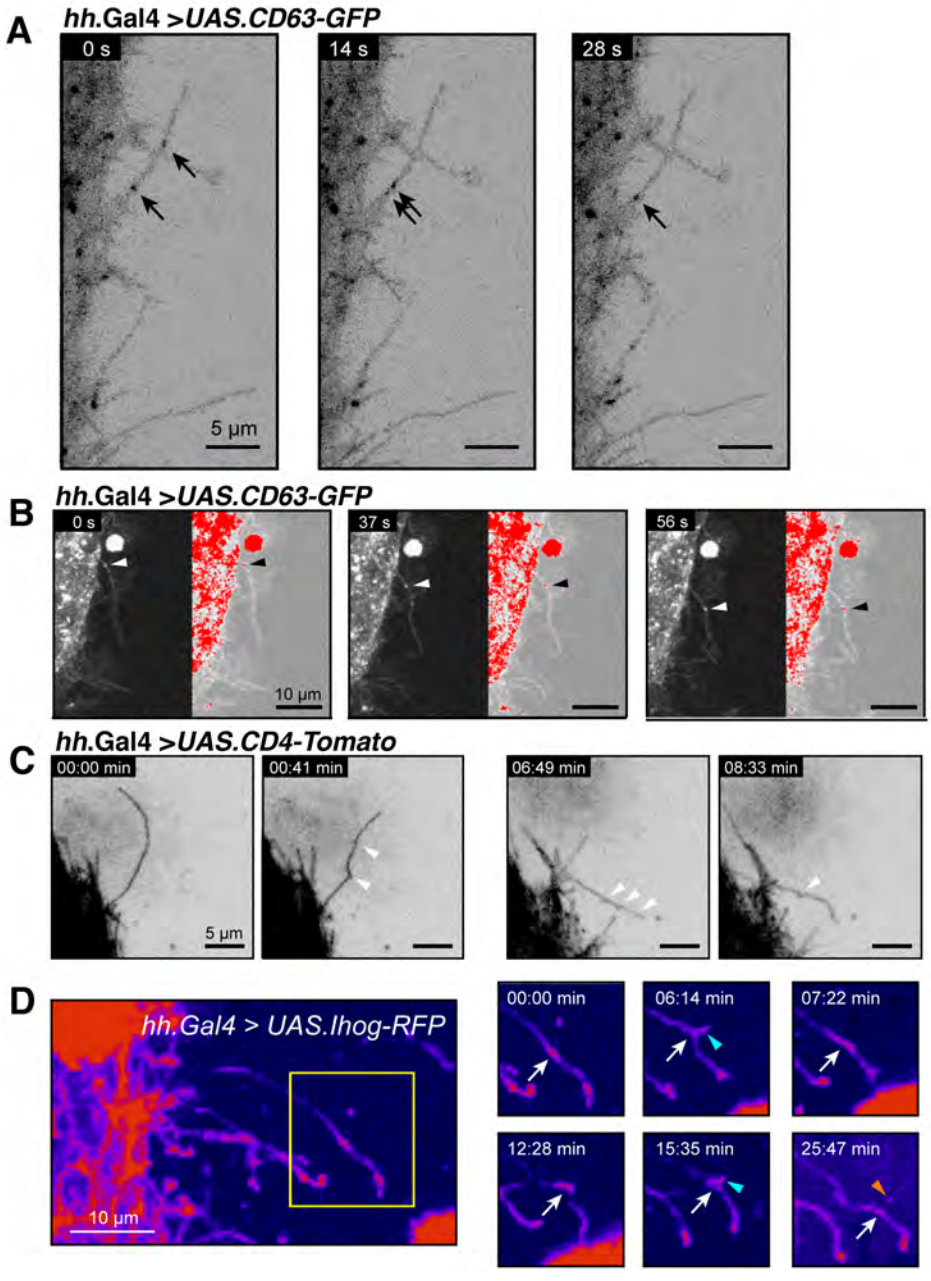
A
hh.Gal4 >UAS.CD63-GFP
0 s
14 s
28 s
5 µm
B
hh.Gal4 >UAS.CD63-GFP
0 s
37 s
56 s
10 µm
C
hh.Gal4 >UAS.CD4-Tomato
00:00 min
00:41 min
06:49 min
08:33 min
5 µm
D
hh.Gal4 > UAS.lhog-RFP
10 µm
00:00 min
06:14 min
07:22 min
12:28 min
15:35 min
25:47 min

**Figure 4**

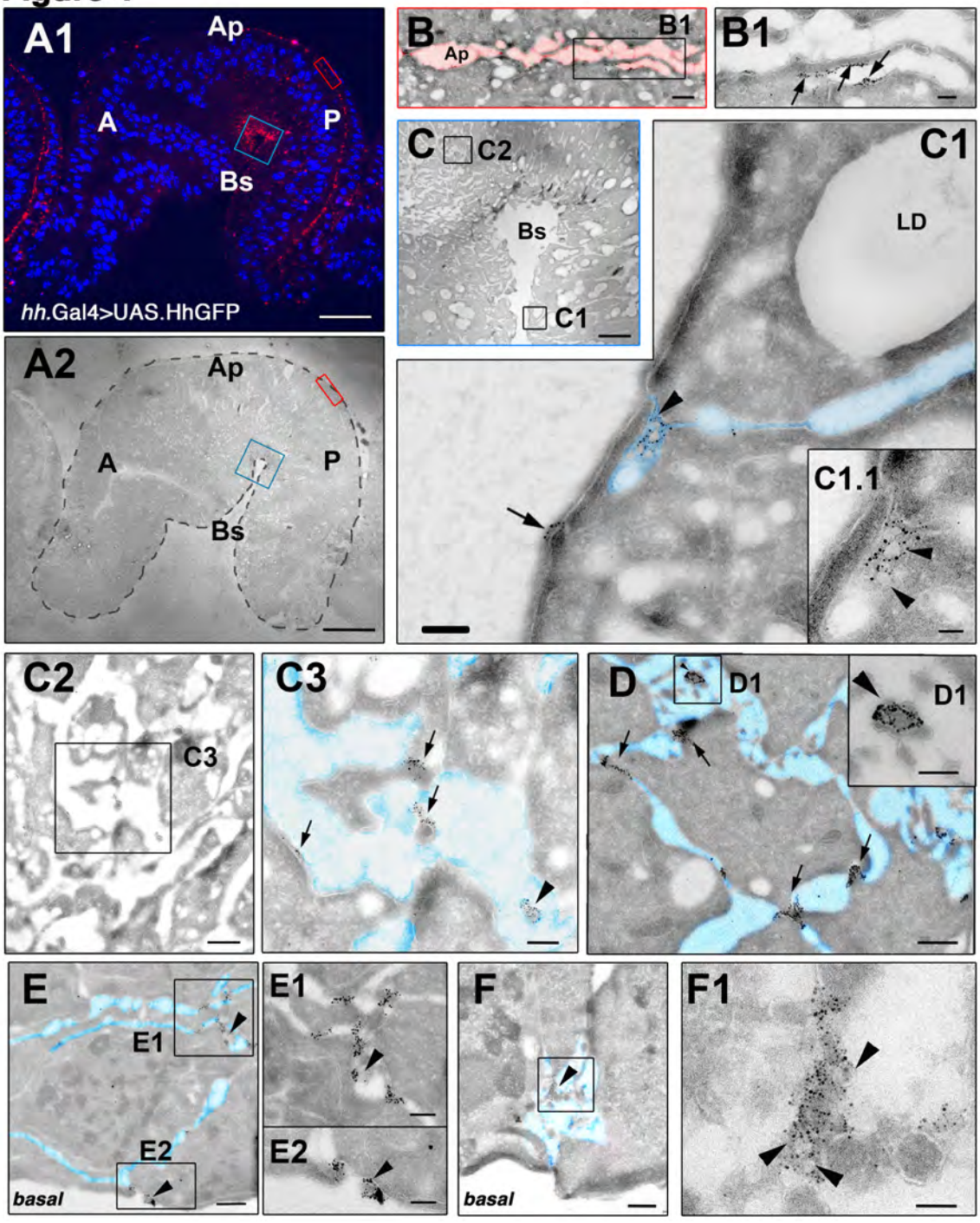
A1
Ap
A
P
Bs
hh.Gal4>UAS.HhGFP
A2
Ap
A
P
Bs
B
B1
Ap
B1
C
C2
Bs
C1
C1
LD
C1.1
C2
C3
C3
D
D1
D1
E
E1
E2
basal
E1
E2
F
basal
F1

# Figure 5

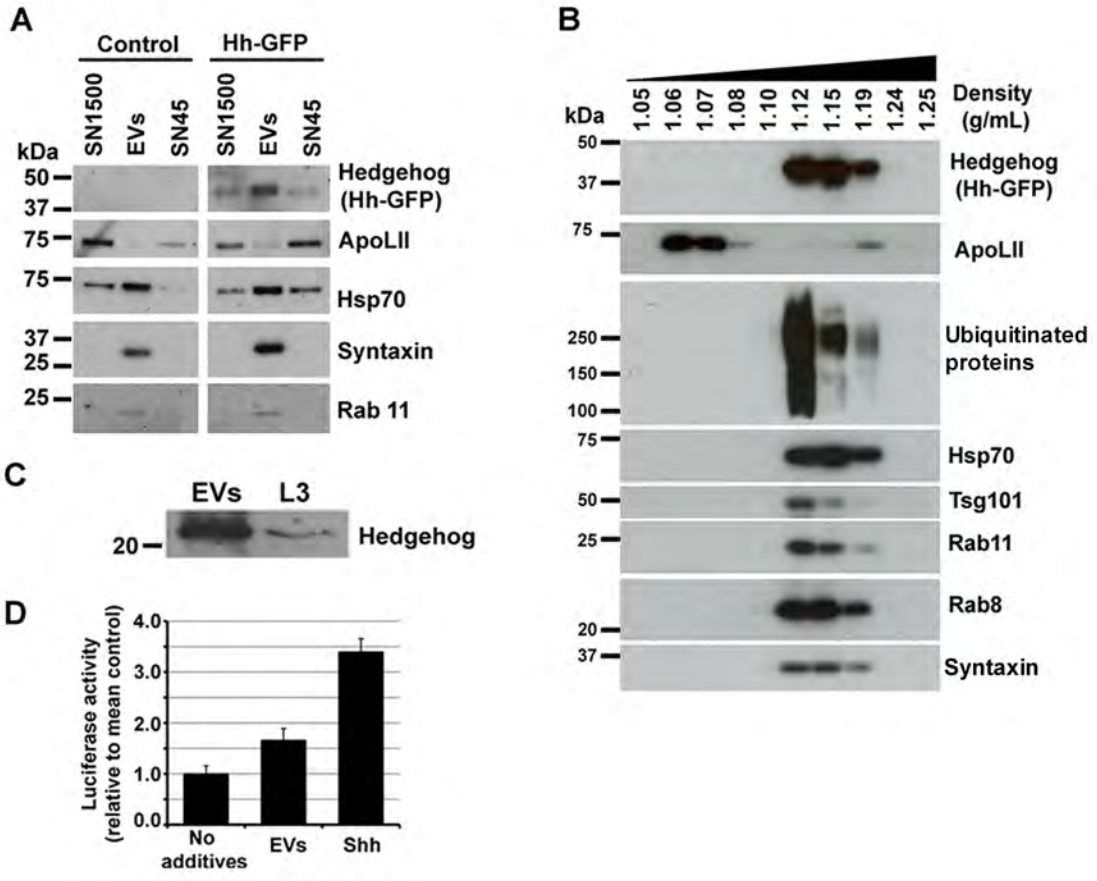
A
Control
Hh-GFP
SN1500
EVs
SN45
SN1500
EVs
SN45
kDa
50
37
75
75
37
25
25
Hedgehog (Hh-GFP)
ApoLII
Hsp70
Syntaxin
Rab 11
B
kDa
1.05
1.06
1.07
1.08
1.10
1.12
1.15
1.19
1.24
1.25
Density (g/mL)
50
37
75
250
150
100
75
50
25
20
37
Hedgehog (Hh-GFP)
ApoLII
Ubiquitinated proteins
Hsp70
Tsg101
Rab11
Rab8
Syntaxin
C
EVs
L3
20
Hedgehog
D
Luciferase activity (relative to mean control)
4.0
3.0
2.0
1.0
0.0
No additives
EVs
Shh

# Figure 6

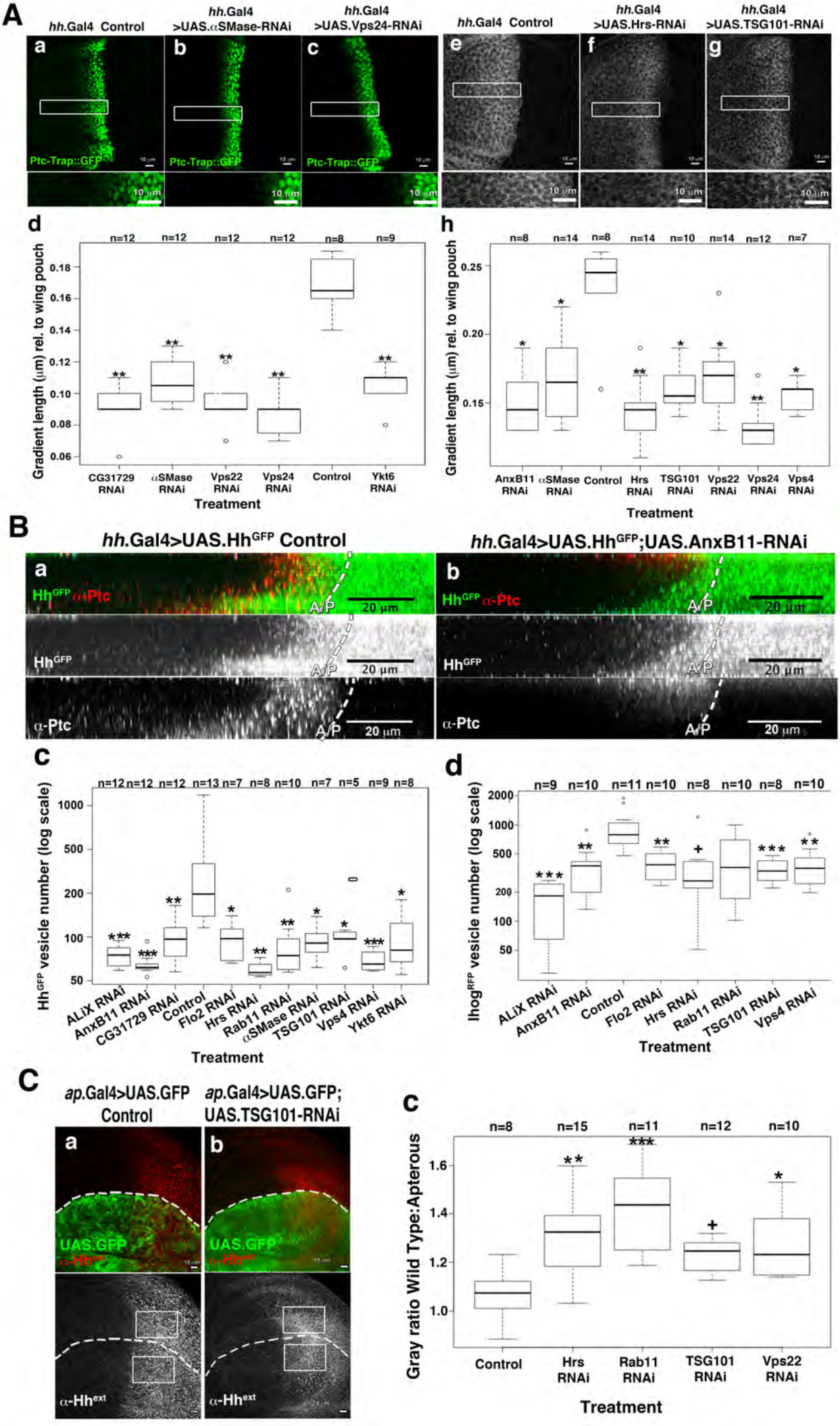
A
hh.Gal4 Control
hh.Gal4 >UAS.αSMase-RNAi
hh.Gal4 >UAS.Vps24-RNAi
hh.Gal4 Control
hh.Gal4 >UAS.Hrs-RNAi
hh.Gal4 >UAS.TSG101-RNAi
a
b
c
e
f
g
Ptc-Trap::GFP
10 μm
d
Gradient length (μm) rel. to wing pouch
n=12 n=12 n=12 n=12 n=8 n=9
CG31729 RNAi
αSMase RNAi
Vps22 RNAi
Vps24 RNAi
Control
Ykt6 RNAi
Treatment
h
n=8 n=14 n=8 n=14 n=10 n=14 n=12 n=7
AnxB11 RNAi
αSMase RNAi
Control
Hrs RNAi
TSG101 RNAi
Vps22 RNAi
Vps24 RNAi
Vps4 RNAi
Treatment
B
hh.Gal4>UAS.HhGFP Control
hh.Gal4>UAS.HhGFP;UAS.AnxB11-RNAi
HhGFP α-Ptc
HhGFP
α-Ptc
A/P
20 μm
c
HhGFP vesicle number (log scale)
n=12 n=12 n=12 n=13 n=7 n=8 n=10 n=7 n=5 n=9 n=8
ALiX RNAi
AnxB11 RNAi
CG31729 RNAi
Control
Flo2 RNAi
Hrs RNAi
Rab11 RNAi
αSMase RNAi
TSG101 RNAi
Vps4 RNAi
Ykt6 RNAi
Treatment
d
lhogRFP vesicle number (log scale)
n=9 n=10 n=11 n=10 n=8 n=10 n=8 n=10
ALiX RNAi
AnxB11 RNAi
Control
Flo2 RNAi
Hrs RNAi
Rab11 RNAi
TSG101 RNAi
Vps4 RNAi
Treatment
C
ap.Gal4>UAS.GFP Control
ap.Gal4>UAS.GFP; UAS.TSG101-RNAi
a
b
UAS.GFP
α-Hhext
c
Gray ratio Wild Type:Apterous
n=8 n=15 n=11 n=12 n=10
Control
Hrs RNAi
Rab11 RNAi
TSG101 RNAi
Vps22 RNAi
Treatment

**SUPPLEMENTARY MATERIAL**

**Supplementary Fig. 1: Ultrastructural localization of Hh, Ihog and Disp in wing discs.** A) Thawed 200 nm thick cryosections of wing disc expressing $Hh^{GFP}$ were immunostained with an anti-GFP antibody followed by a fluorescent (Alexa594) conjugated antibody and nuclear DAPI staining. $Hh^{GFP}$ signal is localized along the apical lumen as well as in the basolateral region of the P compartment. B, C, D, E, F, f) Correlative immunogold labelling of 100 nm thick cryosections with an anti-Hh antibody followed by protein A gold (15nm). Labelling decorated the apical microvilli along the entire disc lumen (arrows in B) as well as basolateral membranes (arrows in C and D), multivesicular bodies (MVB in C and E) and lysosomes in the Hh producing cells (C). Hh staining appears also associated with exovesicle-like structures (F, f) in basolateral spaces (depicted with blue colour in F). G, H) Immunogold labelling of cryosections of wing discs expressing $Ihog^{CFP}$. Staining was performed with an anti-GFP antibody followed by protein A gold (15 nm). Labelling decorated MVBs (G) and exovesicles (arrowheads in G and H-h) at basolateral spaces. Note that in panel H, the basolateral space between adjacent cells (N indicates their nuclei) has been depicted in blue colour to better visualize gold-decorated exovesicles. I) Double-immunogold labelling of Hh and Disp on cryosections of wing disc expressing $Disp^{YFP}$. Labelling was performed with rabbit anti-Hh and guinea pig anti-Disp antibodies followed by 15nm gold conjugated anti-rabbit and 10-nm gold conjugated anti-guinea pig antibodies. Image shows double-labelled on basolateral membranes, MVBs and exovesicles (arrowheads) at basolateral spaces. Bars, 500 nm (F, H) and 200 nm (B,C,D,f,G,I). A and P compartments are indicated in A. Basolateral extracellular spaces are depicted in blue.

**Supplementary Fig. 2: Hedgehog and Ihog are in EVs dependent of the ESCRT complex. A)** Western-blotting of three independent experiments of transfection in Cl8 cells with a vector carrying Hh-GFP. 1/30th of 1% Triton X-100-lysed cells, 1/5th of the purified EVs and 1/350th of

the SN1500 and SN45 were analysed by Western-blotting using antibody against Hedgehog. Both, low and high exposures of the films are indicated in order to visualize the protein in all the fractions. B) Western blotting of cell extracts and purified EVs obtained from untransfected and S2 stably-expressing Hh-GFP cells. Equal amounts of proteins (20 ug) of 1% Triton X-100-lysed cells and of purified EVs were analysed using antibodies against indicated proteins. Note that while a tiny band was observed in cell extract of Hh-GFP expressing cells a clear band was observed in the EVs from Hh-GFP expressing cells indicating an enrichment of Hh-GFP protein in the extracellular vesicular fraction regarding the intracellular Hh content. **C)** Gradient density analysis of EVs from Hh-GFP stably-expressing S2 cells. EVs were fractionated by continuous sucrose density gradient and equal amounts (1/5th) of the resulting fractions analysed by Western blotting. Specific antibodies show the presence of Hh, iHog and exosomal marker Rab11 mapping at similar densities. D) dsRNA treatment against nSMase, TSG101 or Rab27 in *Drosophila* cultured cells Cl8.

**Supplementary Fig. 3: Methods for the quantification of puncta in the A compartment**. A-a) Maximum intensity projection of Z stacks from a wing disc expressing Ihog$^{RFP}$ (control), showing the rectangular area used for quantifications of the number of puncta in the A compartment, a) Image showing the selection used for quantification after delimiting the edge of the P compartment cells. a) Small numbers are the actual quantification showed here in a projection of the Z stacks. B-b) Example of another quantification for one of the RNAi treatments co-expressing Ihog$^{RFP}$, showing the same image analysis procedure as in the control (A). All quantifications were performed per z-slice rather than using projections. C) Confocal sections of wing discs expressing HH$^{GFP}$ in the P compartment (*hh*.Gal4) and immuno-labelled for the receptor Ptc in the A compartment. Yellow line shows the delimitation of the edge obtained after blurring the projected image of all sections. Note how the delimiting line coincides with the compartment border marked by Ptc in red (c).

**Supplementary Fig. 4: Results are robust to controls for RNAi treatments** A) Imaginal discs immunostained with anti-Caspase-3 antibody to analyse the effect of a possible cell death after RNAi treatments (b-d) when compared to a non-treated $Hh^{GFP}$ expressing disc (a). Note that there is no significant increment in cell death. Bars,10 μm. B) Boxplot showing RNA levels after RTcPCR quantification in larvae expressing RNAi treatments and tested for their target genes. Note that there is a significant reduction in specific RNA levels when treated (See Methods). C) *Immuno*staining for total Hh in wild type discs (a) or in wing disc expressing RNAi treatment for AnxB11 (b) driven by *ap.Gal4* with a dorsal expression domain (marked by GFP), leaving the ventral domain in Wild Type conditions as an internal control. Note there is no change in fluorescence levels at the dorsal posterior compartment compared to the ventral side (a,b). (c) Boxplot showing the ratio between relative intensity of the mean gray value in the dorsal (RNAi treated) versus the ventral compartment (Wild type). The ratio is close to 1 in control, and in all RNAi cases except TSG101 and Vps22 where the ratio decreases due to accumulation of Hh in the RNAi treated cells.

Significance levels for pairwise tests (Tukey HSD or Wilcoxon, depending on Normality of data): *** P<0.001, ** P<0.01, *P<0.05, + P<0.1. Bars,10 μm.

**Supplementary Fig. 5: Original films for all Western Blot experiments.** A-C) Western Blots for co-immunprecipitation experiment (Fig. 2 C-E) incubated with antibodies against GFP (A), RFP( B) and Hh (C). D) Western Blots for the isolation of EVs showing Hh, ApoLII in EVs with exosomal markers (Fig. 5A). E) Western Blots for the fractionation of EVs by density gradient showing Hh, ApoLII and exosomal markers (Fig. 5B). F) Western Blots for the isolation of EVs showing $Hh^{GFP}$ (Supplementary Fig. 2A). G) Western Blots for the isolation of EVs showing $Hh^{GFP}$ and Ihog in EVs with exosomal markers (Supplementary Fig. 2B). H) Western Blots for the fractionation of EVs by density gradient showing $Hh^{GFP}$ and Ihog with the exosomal marker

Rab11 (Supplementary Fig. 2C). I) Western Blots for silencing experiments showing EVs with Hh and Syntaxin after dsRNA treatment against nSMase, TSG101 or Rab27 in *Drosophila* cultured cells Cl8 (Supplementary Fig. 2D). Thus WB was also used to show endogenous Hh (Vehicle lane) in EVs with a control for Hh expression from Larvae extracts (Fig. 5C)

**Supplementary Movies**

To observe all the details in these complex Movies, please use the arrow keys to play the Movies in Quicktime (Apple, Inc.). In all Movies, anterior is to the left.

**Supplementary Movie 1:** 3D Reconstruction of a *z*-stack from apical to basal of a *hh.Gal4>UAS.Ihog$^{RFP}$; UAS.Hh$^{GFP}$ wing disc.* Movie shows a disc rotated from above apical side to a lateral side. Note the presence of vesicles all along the lateral side and along cytonemes at the basal part of the disc. Bar,10 μm.

**Supplementary Movie 2.** Ihog$^{RFP}$ labels cytonemes and punctate structures in the abdominal epidermis *in vivo*. Histoblasts of the P compartment are labelled with *hh.Gal4>UAS.Ihog$^{RFP}$*. Lateral region of the epithelium shown in the top panel and basal region in the bottom panel. Note that besides the basal cytonemes, which reach into the A compartment, punctate structures can be found in the A compartment both basally and laterally. Bar, 10 μm. Anterior is to the left.

**Supplementary Movie 3**. Punctate structures labelled with CD63$^{GFP}$ co-localize with those labelled with Ihog$^{RFP}$ *in vivo*. Cells of the P compartment are labelled with hh.*Gal4 >UAS.CD63-GFP, UAS.Ihog$^{RFP}$*. The white arrow highlights a protrusion, in which puncta are most noticeable. Bar, 5 μm.

**Supplementary Movie 4**. Punctate structures labelled with CD63$^{GFP}$ move along cytonemes *in vivo*. Cells of the P compartment are labelled with hh.*Gal4 >UAS.CD63$^{GFP}$*. The white arrow highlights a protrusion, in which puncta are most noticeable. Bar, 5 μm.

**Supplementary Movie 5**. Punctate structures labelled with CD63$^{GFP}$ move along cytonemes *in*

*vivo*. Cells of the P compartment are labelled with hh.*Gal4 >UAS.CD63$^{GFP}$*. Arrowheads highlight puncta, which move along a protrusion. Fluorescence is depicted using a grey (left) and a HiLo lookup table (right), which highlights the brightest pixels in red. Bar, 10 µm.

**Supplementary Movie 6**. Cytonemes labelled with CD4-Tomato show 'buckling' and 'swelling'. The first arrows highlight 'buckles', the later ones 'swellings'. Cells of the P compartment are labelled with hh.*Gal4 >UAS.CD4-Tomato*. Fluorescence is depicted using an inverted grey lookup table. Bar, 5 µm.

**Supplementary Movie 7**. Ihog$^{RFP}$ puncta move along cytonemes. P compartment cells and their cytonemes are labelled with *hh.Gal4 >UAS.Ihog$^{RFP}$* and coloured with a Fire lookup table. Note punctate structures, which are located along the cytonemes (white arrows). One punctum is budding and finally shedding from the cytoneme (cyan arrow indicates punctum shortly before it leaves the protrusion). Note also that Ihog$^{RFP}$ labels puncta, which are not associated to cytonemes. Bar, 10 $\mu$ m.

# Supplementary Figure 2

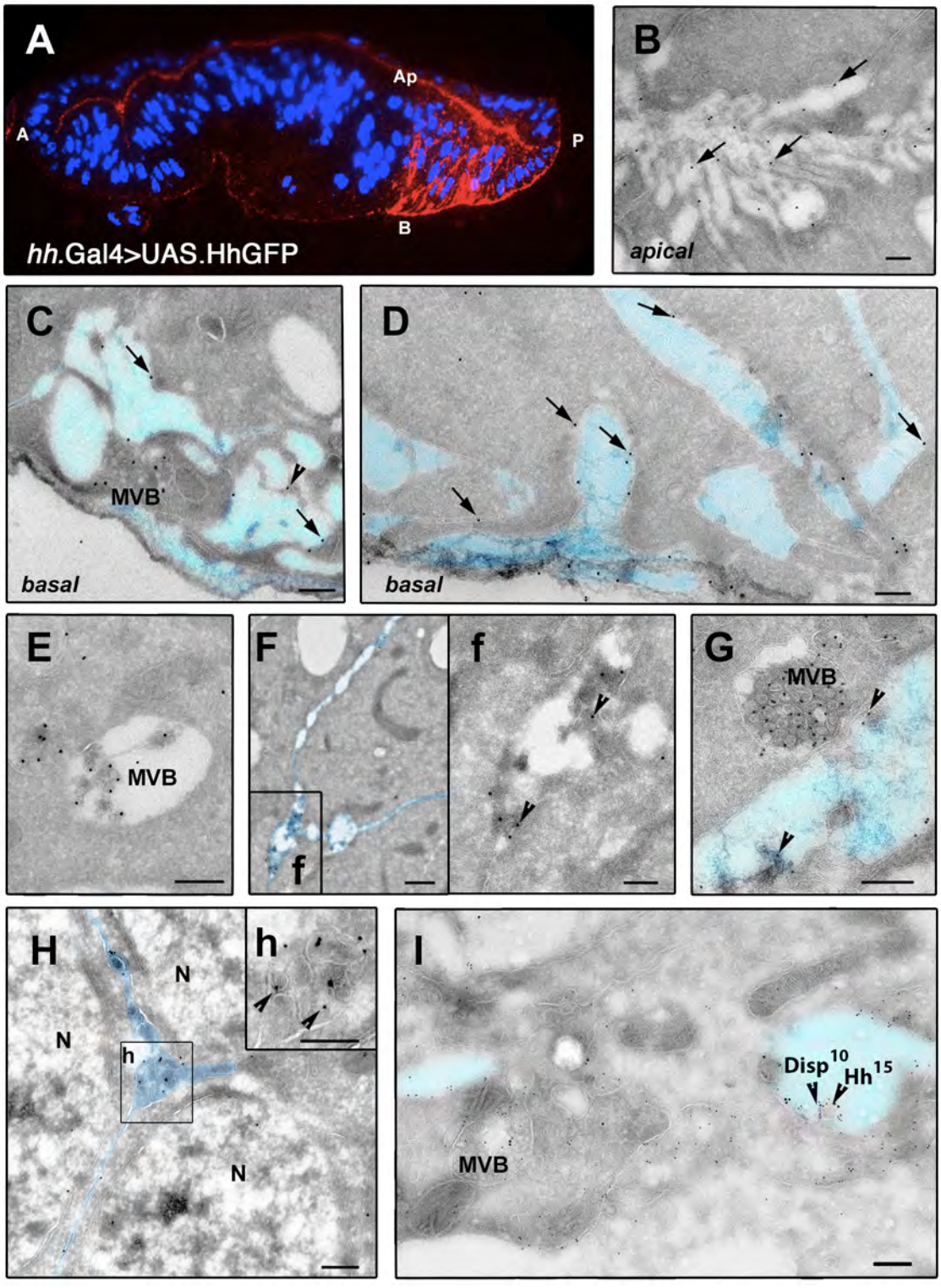

## Supplementary Figure 2

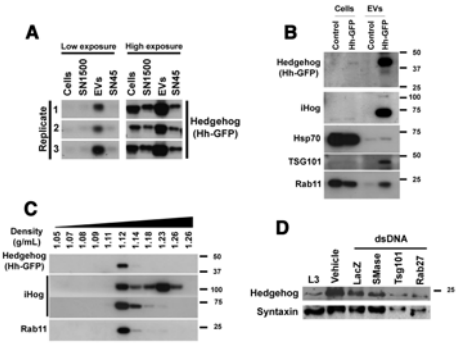

# Supplementary Figure 3

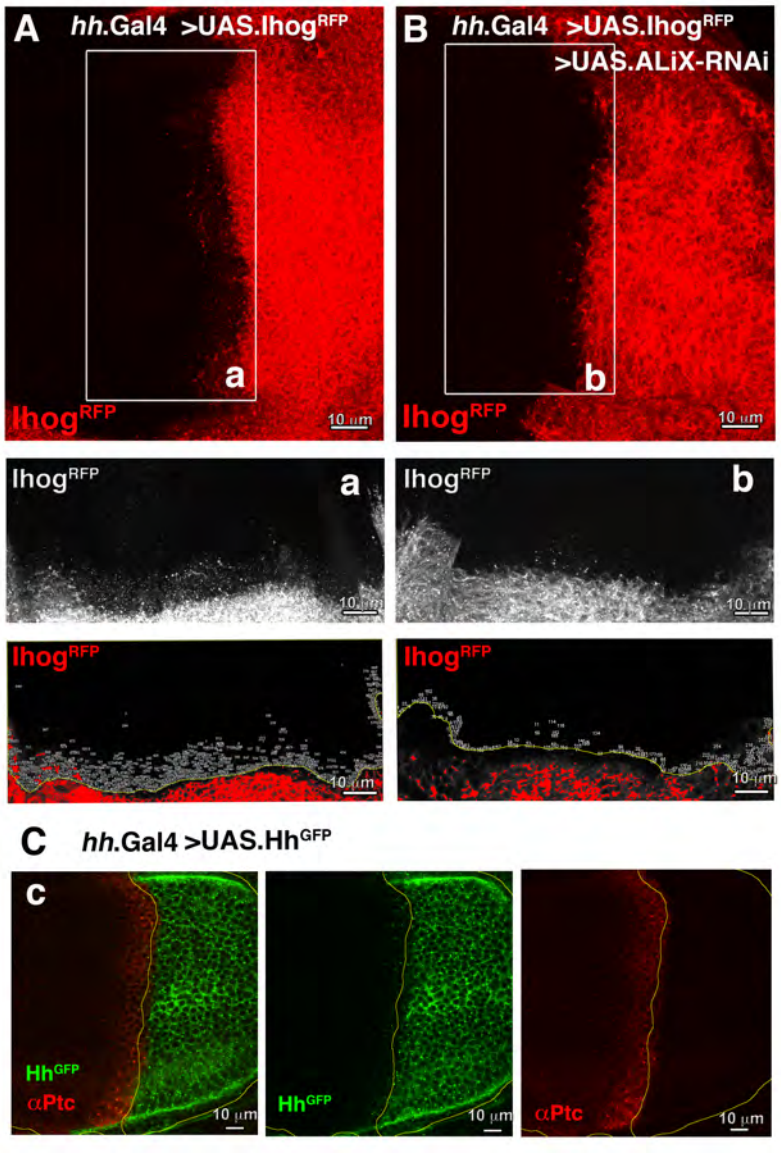

# Supplementary Figure 4

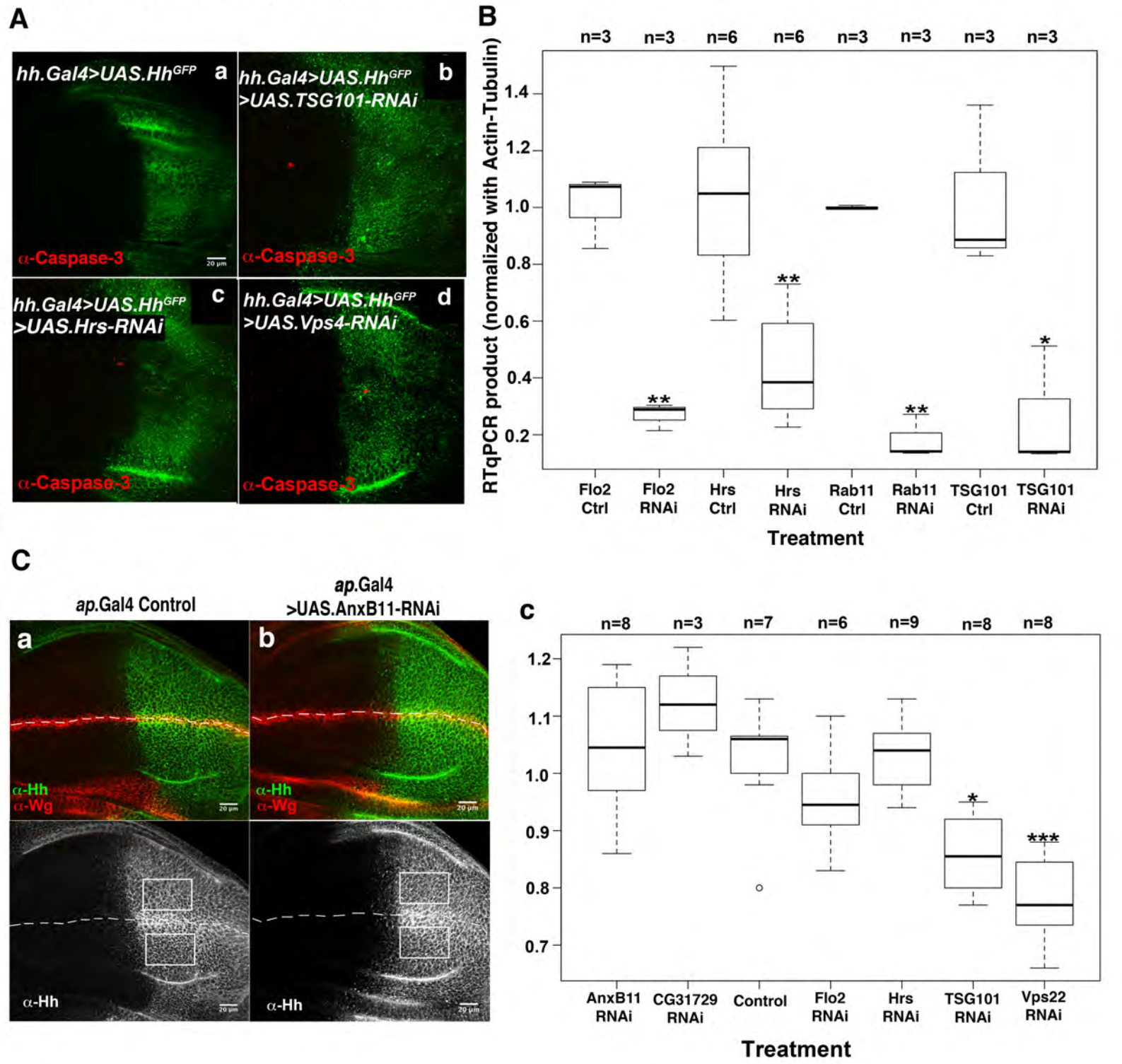

# Supplementary Figure 5

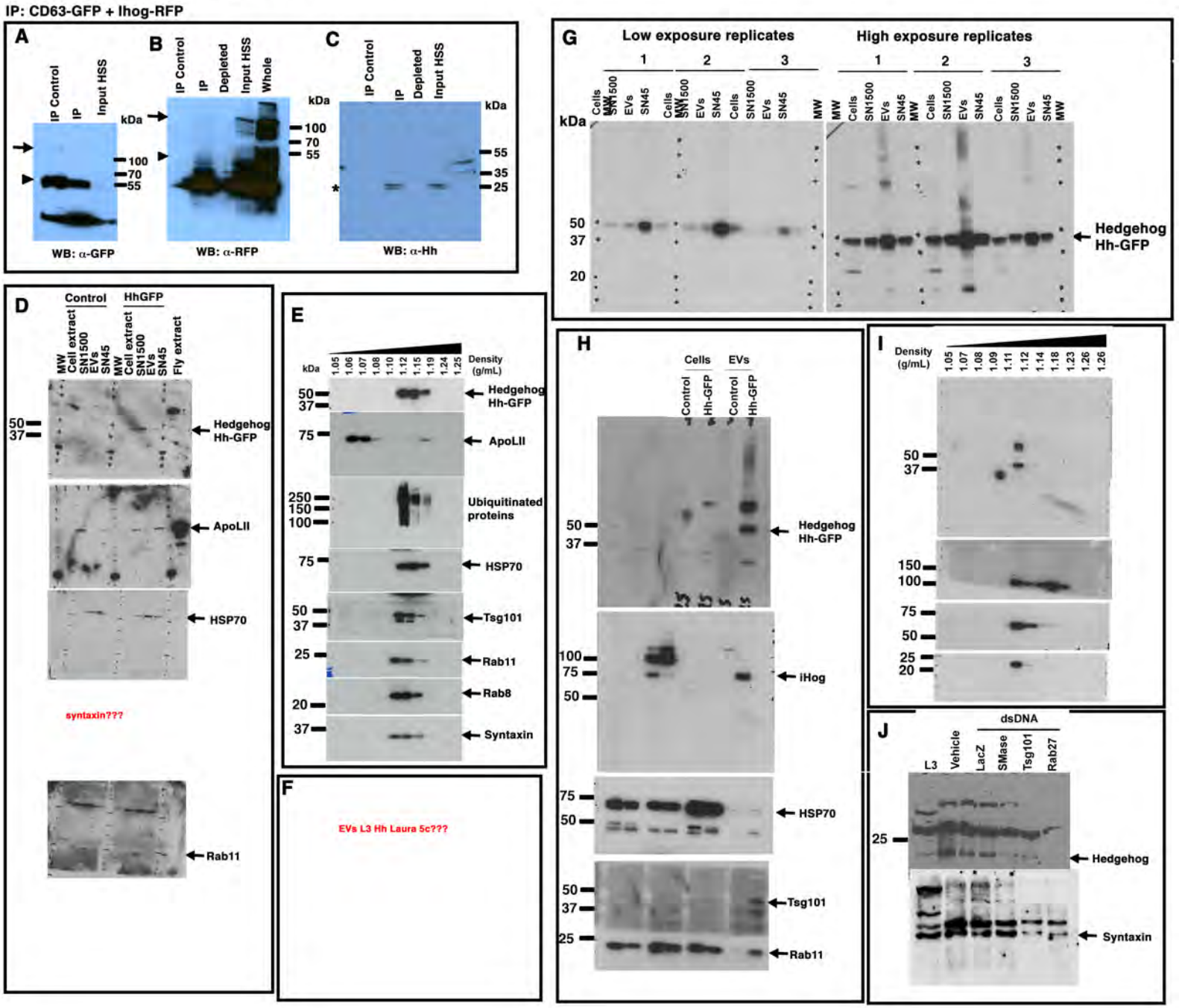

**Supplementary Table 1: *Drosophila* stocks**

| Name (Symbol) | TYPE | Procedence Stock Number | FlyBase ID (stock) | FlyBase ID (gene) | Annotation symbol |
|---|---|---|---|---|---|
| **ALG-2 interacting protein X (ALiX)** | UAS-RNAi line | Bloomington Drosophila Stock Center #33417 | FBst0033417 | FBgn0086346 | CG12876 |
| **Annexin B11 (AnxB11)** | UAS-RNAi line | Vienna *Drosophila* RNAi Centre #29693 | FBst0458097 | FBgn0030749 | CG9968 |
| **Flotillin 2 (Flo2)** | UAS-RNAi line | Vienna *Drosophila* RNAi Centre #31525 | FBst0459071 | FBgn0264078 | CG32593 |
| **Hepatocyte growth factor regulated tyrosine kinase substrate (Hrs)** | UAS-RNAi line | Bloomington Drosophila Stock Center #33900 | FBst0033900 | FBgn0031450 | CG2903 |
| **Rab11 (Rab11)** | UAS-RNAi line | Vienna *Drosophila* RNAi Centre #108382 | FBst0480193 | FBgn0015790 | CG5771 |
| **αSMase** | UAS-RNAi line | Bloomington Drosophila Stock Center #25283 | FBst0025283 | FBgn0039769 | CG15534 |
| **Tumor susceptibility gene 101 (TSG101)** | UAS-RNAi line | Bloomington Drosophila Stock Center #35710 | FBst0035710 | FBgn0036666 | CG9712 |
| **Vacuolar protein sorting 4 (Vps4)** | UAS-RNAi line | Vienna *Drosophila* RNAi Centre #105977 | FBst0477803 | FBgn0027605 | CG6842 |
| **Larsen (Vps22)** | UAS-RNAi line | Bloomington Drosophila Stock Center #38289 | FBst0038289 | FBgn0260940 | CG6637 |
| **Vacuolar protein sorting 24 (Vps24)** | UAS-RNAi line | Bloomington Drosophila Stock Center #38281 | FBst0038281 | FBgn0037231 | CG9779 |
| **YKT6 ortholog (S. cerevisiae) (Ykt6)** | UAS-RNAi line | Bloomington Drosophila Stock Center #38314 | FBst0038314 | FBgn0260858 | CG1515 |

| | | | | | |
|---|---|---|---|---|---|
| **Cation–transporting P-type ATPase (TAT-5)** | UAS-RNAi line | Vienna *Drosophila* RNAi Centre #105987 | FBst0477813 | FBgn0051729 | CG31729 |
| **Hedgehog** | UAS-HhGFP | Torroja et al., 2004 | FBtp0019401 | FBgn004644 | CG4637 |
| **Ihog** | UAS-IhogRFP<br>UAS-IhogYFP<br>UAS-IhogCFP | Bilioni et al., 2013<br><br>Callejo et al., 2011 | FBtp0083037 | FBgn0031872 | CG9211 |
| **Apterus** | Gal4 | Bloomington Drosophila Stock Center #56807 | FBst0056807 | FBgn0000099 | CG8376 |
| **α-Tubulin at 84B** | Gal4 | Bloomington Drosophila Stock Center #30036 | FBst0030036 | FBgn0003884 | CG1913 |
| **CD-63** | UAS-CD63GFP | Panakova et al., 2005 | FBtp0020578 | FBtp0020578 | ENSG00000135404 |
| **Dispatched** | UAS-Disp<br><br>UAS-DispYFP | Burke et al., 1999<br>Callejo et al., 2011 | FBtp0011804<br><br>FBtp0083034 | FBgn0029088 | CG2019 |
| **Patched** | Promoter enhancer trap-GFP (Spradling) | DGRC | Fly Trap GFP CB02030 | FBgn0003892 | CG2411 |
| **Hedgehog** | Gal4 | Takei et al., 2004 | FBti0017278 | FBgn004644 | CG4637 |
| **GFP** | UAS-EGFP | Bloomington Drosophila Stock Center #5430 | FBst0005430 | FBtp0011396 | |
| **CD-4** | UAS-CD4-Tomato | Han et al., 2011 | FBtp0068019 | FBgn0263317 | ENSG00000010610 |